Lyα Emission-Line Galaxies at $z = 3.1$ in the Extended Chandra Deep Field South

Caryl Gronwall, Robin Ciardullo, Thomas Hickey

Department of Astronomy & Astrophysics, The Pennsylvania State University
525 Davey Lab, University Park, PA 16802

caryl@astro.psu.edu, rbc@astro.psu.edu, tomhickey@astro.psu.edu

Eric Gawiser[1]

Yale Astronomy Department and Yale Center for Astronomy and Astrophysics
Yale University, P.O. Box 208121, New Haven, CT 06520

gawiser@astro.yale.edu

John J. Feldmeier[1]

Department of Physics & Astronomy, Youngstown State University, Youngstown, OH 44555-2001

jjfeldmeier@ysu.edu

Pieter G. van Dokkum, C. Megan Urry, David Herrera

Yale Astronomy Department and Yale Center for Astronomy and Astrophysics and Yale Physics Department
Yale University, P.O. Box 208121, New Haven, CT 06520

pieter.vandokkum@yale.edu, meg.urry@yale.edu, david.herrera@yale.edu

Bret D. Lehmer

Department of Astronomy & Astrophysics, The Pennsylvania State University
525 Davey Lab, University Park, PA 16802

blehmer@astro.psu.edu

Leopoldo Infante, Alvaro Orsi

Departmento de Astronomía y Astrofísica, Pontificia Universidad Católica de Chile, Casilla 306, Santiago 22, Chile

linfante@astro.puc.cl, aaorsi@astro.puc.cl

Danilo Marchesini

Yale Astronomy Department and Yale Center for Astronomy and Astrophysics
Yale University, P.O. Box 208121, New Haven, CT 06520

danilom@astro.yale.edu

Guillermo A. Blanc

Astronomy Department, University of Texas, Austin, TX 78712

gblancm@astro.as.utexas.edu

Harold Francke, Paulina Lira

Departamento de Astronomía, Universidad de Chile, Casilla 36-D, Santiago, Chile

hfrancke@das.uchile.cl, plira@das.uchile.cl

and

Ezequiel Treister

European Southern Observatory, Casilla 19001, Santiago, Chile

etreiste@eso.org

ABSTRACT

We describe the results of an extremely deep, 0.28 deg^2 survey for $z = 3.1$ Lyα emission-line galaxies in the Extended Chandra Deep Field South. By using a narrow-band 5000 Å filter and complementary broadband photometry from the MUSYC survey, we identify a statistically complete sample of 162 galaxies with monochromatic fluxes brighter than 1.5×10^{-17} ergs cm^{-2} s^{-1} and observers frame equivalent widths greater than 80 Å. We show that the equivalent width distribution of these objects follows an exponential with a rest-frame scale length of $w_0 = 76^{+11}_{-8}$ Å. In addition, we show that in the emission line, the luminosity function of Lyα galaxies has a faint-end power-law slope of $\alpha = -1.49^{+0.45}_{-0.34}$, a bright-end cutoff of $\log L^* = 42.64^{+0.26}_{-0.15}$, and a space density above our detection

[1]NSF Astronomy and Astrophysics Postdoctoral Fellow

thresholds of $1.46 \pm 0.12 \times 10^{-3}\, {h_{70}}^{3}$ galaxies Mpc^{-3}. Finally, by comparing the emission-line and continuum properties of the LAEs, we show that the star-formation rates derived from Lyα are ~ 3 times lower than those inferred from the rest-frame UV continuum. We use this offset to deduce the existence of a small amount of internal extinction within the host galaxies. This extinction, coupled with the lack of extremely-high equivalent width emitters, argues that these galaxies are not primordial Pop III objects, though they are young and relatively chemically unevolved.

Subject headings: cosmology: observations – galaxies: formation – galaxies: high-redshift – galaxies: luminosity function

1. Introduction

The past decade has seen an explosion in our ability to detect and study $z > 3$ galaxies and probe the history of star formation in the universe (e.g., Madau et al. 1996). This has been mostly due to the development of the Lyman-break technique, whereby high redshift galaxies are identified via a flux discontinuity caused by Lyman-limit absorption (see Steidel et al. 1996a,b). By taking deep broadband images, and searching for U, B, and V-band dropouts, astronomers have been able to explore large-scale structure and determine the properties of bright ($L > 0.3L^*$) galaxies between $z \sim 3$ and $z \sim 5$ (Giavalisco 2002).

The stunning success of the Lyman-break technique stands in contrast to the initial results of Lyα emission-line observations. The failure of the first generation of these surveys (e.g., De Propis et al. 1993; Thompson, Djorgovski, & Trauger 1995) was attributed to internal extinction in the target galaxies (Meier & Terlevich 1981). Since Lyα photons are resonantly scattered by interstellar hydrogen, even a small amount of dust can reduce the emergent emission-line flux by several orders of magnitude.

Fortunately, Lyα surveys have recently undergone a resurgence. Starting with the Keck observations of Cowie & Hu (1998) and Hu, Cowie, & McMahon (1998), narrow-band searches for Lyα emission have been successfully conducted at a number of redshifts, including $z \sim 2.4$ (Stiavelli et al. 2001), $z \sim 3.1$ (Ciardullo et al. 2002; Hayashino et al. 2004; Venemans et al. 2005; Gawiser et al. 2006a), $z \sim 3.7$ (Fujita et al. 2003), $z \sim 4.5$ (Rhoads et al. 2000), $z \sim 4.9$ (Ouchi et al. 2003), $z \sim 5.7$ (Rhoads et al. 2003; Ajiki et al. 2003; Tapken et al. 2006), and $z \sim 6.5$ (Kodaira et al. 2003; Taniguchi et al. 2005). The discovery of these high-redshift Lyα emitters (LAEs) has opened up a new frontier in astronomy. At $z > 4$, LAEs are as easy to detect than Lyman-break galaxies (LBG), and, by

$z > 6$, they are the only galaxies observable from the ground. By selecting galaxies via their Lyα emission, it is therefore possible to probe much further down the galaxy continuum luminosity function than with the Lyman-break technique, and perhaps identify the most dust-free objects in the universe. In addition, by using Lyα emitters as tracers of large-scale structure (Steidel et al. 2000; Shimasaku et al. 2004), it is possible to efficiently probe the expansion history of the universe with a minimum of cosmological assumptions (e.g., Blake & Glazebrook 2003; Seo & Eisenstein 2003; Koehler et al. 2007).

Here, we describe the results of a deep survey for Lyα emission-line galaxies in a 0.28 deg^2 region centered on the Extended Chandra Deep Field South (ECDF-S). This region has an extraordinary amount of complementary data, including high-resolution optical images from the *Hubble Space Telescope* via the Great Observatories Origins Deep Survey (GOODS; Giavalisco et al. 2004) and the Galaxy Evolution from Morphology and SEDs program (GEMS; Rix et al. 2004), deep groundbased $UBVRIzJHK$ photometry from the Multiwavelength Survey by Yale-Chile (MUSYC; Gawiser et al. 2006b), mid- and far-IR observations from *Spitzer,* GOODS and MUSYC, and deep X-ray data from *Chandra* (Giacconi et al. 2002; Alexander et al. 2003; Lehmer et al. 2005). In Section 2, we describe our observations, which include over 28 hours worth of exposures through a narrow-band filter on the CTIO 4-m telescope. We also review the techniques used to detect the emission-line galaxies, and discuss the difficulties associated with analyzing samples of LAEs discovered via fast-beam instruments. In Section 3, we describe the continuum properties of our Lyα emitters, including their rest-frame $m_{1050} - m_{1570}$ colors, and compare their space density to that of Lyman-break galaxies. In Section 4, we examine the LAE's equivalent width distribution and show that our sample contains very few of the extremely-high equivalent width objects found by Dawson et al. (2004) at $z = 4.5$. In Section 5, we present the Lyα emission-line luminosity function, and give values for its best-fit Schechter (1976) parameters and normalization. In Section 6, we translate these Lyα fluxes into star-formation rates, and consider the properties of LAEs in the context of the star-formation rate (SFR) history of the universe. We conclude by discussing the implications our observations have for surveys aimed at determining cosmic evolution.

For our analysis, we adopt a ΛCDM cosmology with $H_0 = 70$ km s^{-1} Mpc^{-1} ($h_{70} = 1$), $\Omega_M = 0.3$, and $\Omega_\Lambda = 0.7$. At $z = 3.1$, this implies a physical scale of 7.6 kpc per arcsecond.

2. Observations and Reductions

Narrow-band observations of the ECDF-S were performed with the MOSAIC II CCD camera on the CTIO Blanco 4-m telescope. These data consisted of a series of 111 exposures

taken over 16 nights through a 50 Å wide full-width-half-maximum (FWHM) λ5000 filter (see Figure 1). The total exposure time for these images was 28.17 hr; when the effects of dithering to cover for a dead CCD during some of the observations are included, the net exposure time becomes $\sim$ 24 hr. The total area covered in our survey is 998 arcmin^2; after the regions around bright stars are excluded, this area shrinks 993 arcmin^2. The overall seeing on the images is $1\farcs0$. A log of our narrow-band exposures appears in Table 1.

The procedures used to reduce the data, identify line emitters, and measure their brightnesses were identical to those detailed in Ciardullo et al. (2002) and Feldmeier et al. (2003). After de-biasing, flat-fielding, and aligning the data, our narrow-band frames were co-added to create a master image that was clipped of cosmic rays. This frame was then compared to a deep B+V continuum image provided by the MUSYC survey (Gawiser et al. 2006b) in two different ways. First, the DAOFIND task within IRAF was run on the summed narrow-band and continuum image using a series of three convolution kernels, ranging from one matching the image point-spread-function (PSF), to one $\sim$ 3 times larger. This created a source catalog of all objects in our field. These targets were then photometrically measured with DAOPHOT's PHOT routine, and sources with on-band minus continuum colors less than -1.03 in the AB system were flagged as possible emission-line sources (see Figure 2). At the same time, candidate LAEs were also identified by searching for positive residuals on a "difference" image made by subtracting a scaled version of the B+V continuum image from the narrow-band frame. In this case, the DAOFIND algorithm was set to flag all objects brighter than four times the local standard deviation of the background sky (see Figure 3). As pointed out by Feldmeier et al. (2003), these two techniques complement each other, since each detects objects that the other does not. Specifically, $\lesssim 10\%$ of galaxies were missed by the color-magnitude method due to image blending and confusion, but found with the difference method. Conversely, objects at the frame limit that were lost amidst the increased noise of the difference frame, could still be identified via their on-band minus off-band colors.

Finally, because we intentionally biased our DAOFIND parameters to identify faint sources at the expense of false detections, each emission-line candidate was visually inspected on the narrow-band, $B + V$ continuum, and difference frames, as well as two frames made from subsamples of half the on-band exposures. This last step excluded many false detections at the frame limit, and left us with a sample of 259 candidate LAEs for analysis.

Once found, the equatorial positions of the candidate emission-line galaxies were derived with respect to the reference stars of the USNO-A 2.0 astrometric catalog (Monet et al. 1998). The measured residuals of the plate solution were $\sim 0\farcs2$, a number slightly less than the $0\farcs25$ external error associated with the catalog. Relative narrow-band magnitudes for the objects were derived by first measuring the sources with respect to field stars using an

aperture slightly greater than the frame PSF. Since most of the galaxies detected in this survey are, at best, marginally resolved on our 1″ images, this procedure was sufficiently accurate for our purposes. We then obtained standard AB magnitudes by comparing large aperture photometry of the field stars to similar measurements of the spectrophotometric standards Feige 56 and Hiltner 600 (Stone 1977) taken on three separate nights. The dispersion in the photometric zero point computed from our standard star measurements was 0.03 mag.

2.1. Derivation of Monochromatic Fluxes

The fast optics of wide-field instruments, such as the MOSAIC camera at the CTIO 4-m telescope, present an especially difficult challenge for narrow-band imaging. The transmission of an interference filter depends critically on the angle at which it is illuminated: light entering at the normal will constructively/destructively interfere at a different wavelength than light coming in at an angle (Eather & Reasoner 1969). As a result, when placed in a fast converging beam, an interference filter will have its bandpass broadened and its peak transmission decreased by a substantial amount. This effect is important, for without precise knowledge of the filter bandpass, it is impossible to derive accurate monochromatic fluxes or estimate equivalent widths.

To derive the filter transmission, we began with the throughput information provided by the CTIO observatory[1]. This curve, which represents the expected transmission of the [O III] interference filter in the f/3.2 beam of the Blanco telescope, was computed by combining laboratory measurements of the filter tipped at several different angles from the incoming beam (for a discussion of this procedure, see Jacoby et al. 1989). We then shifted this curve 2 Å to the blue, to compensate for the thermal contraction of the glass at the telescope, and compared this model bandpass to the measured emission-line wavelengths obtained from follow-up spectroscopy (Lira et al. 2007). Interestingly, redshift measurements of 72 galaxies detected in three independent MUSYC fields confirm the shape of the filter's transmission curve, but not its central wavelength: according to the spectroscopy, the mean wavelength of the filter is 10 Å bluer than given by CTIO (Gawiser et al. 2007). Examining the source of this discrepancy is beyond the scope of this paper. However, the data do confirm that, when placed in the beam of the CTIO 4-m prime focus MOSAIC camera, the bandpass of the CTIO [O III] interference filter is nearly Gaussian in shape. This bandpass is reproduced in the left-hand panel of Figure 4.

[1]http://www.ctio.noao.edu/instruments/FILTERS/index.html

This non-square bandpass has important consequences for the analysis of large samples of emission-line galaxies. The first of these involves the definition of survey volume. Because the transmission of the filter declines away from the bandpass center, the volume of space sampled by our observations is a strong function of line strength. This is illustrated in the center panel of Figure 4. Objects with bright line emission can be detected even if their redshifts place Lyα in the wings of the filter, hence the volume covered for these objects is realtively large. Conversely, weak Lyα sources must have their line emission near the center of the bandpass to be observable. As a result, the "effective" volume for our integrated sample of galaxies is a function of the galaxy emission-line luminosity function.

A second concern deals with the sample's flux calibration. In order to compare the flux of an emission-line object to that of a spectrophotometric standard star (i.e., a continuum source) one needs to know both the filter's integral transmission and its monochromatic transmission at the wavelength of interest (Jacoby et al. 1987, 1989). When observing objects at known redshift, the latter requirement is not an issue. However, when measuring a set of galaxies which can fall anywhere within a Gaussian-shaped transmission curve, the transformation between an objects' (bandpass-dependent) AB magnitude and its monochromatic flux is not unique. In fact, if we assume that galaxies are (on average) distributed uniformly in redshift space, then the number of emission-line objects present at a given transmission, T, is simply proportional to the amount of wavelength associated with that transmission value. Consequently, the observed distribution of emission-line fluxes will be related to the true distribution via a convolution, whose (unity normalized) kernel, $G(T)$, is

$$G(T)dT = \left\{ \left| \frac{d\lambda}{dT} \right| dT \right\}_{\rm blue} + \left\{ \left| \frac{d\lambda}{dT} \right| dT \right\}_{\rm red} \qquad (1)$$

where the first term describes the filter's response blueward of the transmission peak and the second term gives the response redward of the peak. The center panel of Figure 4 displays this kernel for the filter used in our survey. The curve shows that for roughly half of the detectable galaxies in our field, the effect of our filter's non-square bandpass is minimal. However, for the other $\sim 50\%$ of galaxies, the shape of the bandpass is extremely important, and the inferred fluxes for some objects can be off by over a magnitude.

Any analysis of the ensemble properties of our LAEs must consider the full effect that the non-square bandpass and the odd-shaped convolution kernal has on the sample. We do this in Sections 4 and 5. However, one often wants to quote the monochromatic flux and equivalent width for an *individual* Lyα emitter. To do this, we need to adopt an appropriate "mean" value for the transmission of our filter. The most straightforward way to define this number is via the filter's peak transmission. This is where the survey depth is greatest, and choosing $T_{\rm max}$ is equivalent to assigning each galaxy its "most probable" monochromatic flux.

Unfortunately, by defining the transmission in this way, we underestimate the flux from all galaxies whose line emission does not fall exactly on this peak. Alternatively, we can attempt to choose a transmission which globally minimizes the flux errors of all the galaxies detected in the survey. This can be done by weighting each transmission by the number of galaxies one expects to observe at that wavelength: the greater the transmission, the deeper the survey, and the more galaxies present in the sample. The difficulty with this "expectation value" approach is that it requires prior knowledge of the distribution of emission-line fluxes, which is one of the quantities we are attempting to measure. That leads us to a third possibility: to approximate the filter's expectation value using some "characteristic" transmission, T_C, which is independent of the galaxy luminosity function, but still takes the filter's changing transmission into account. The arrow in Figure 4 identifies the transmission we selected as being characteristic of the filter; the justification for this value is presented in Section 5. We emphasize that T_C is only a convenient mean that enables us to quote the likely emission-line strengths of *individual* galaxies. When analyzing the global properties of an ensemble of LAEs, the full non-Gaussian nature of the filter's convolution kernel must be taken into account.

Using this transmission and our knowledge of the filter curve, we converted the galaxies' AB magnitudes to monochromatic fluxes at $\lambda = 5000$ Å via

$$F_{5000} = 3.63 \times 10^{-20}\, 10^{-m_{\rm AB}/2.5} \cdot \frac{c}{\lambda^2} \cdot \frac{\int T_\lambda d\lambda}{T_C} \tag{2}$$

where F_{5000} is given in ergs cm^{-2} s^{-1} (Jacoby et al. 1987). Equivalent widths then followed via

$$\mathrm{EW} = \frac{F_{5000}}{f_{B+V}} - \Delta\lambda \tag{3}$$

where f_{B+V} is the objects' AB flux density in the $B+V$ continuum image, and $\Delta\lambda$, the FWHM of the narrow-band filter, represents the contribution of the galaxy's underlying continuum within the bandpass. Both these equations are only applicable to objects whose line emission dominates the continuum within the narrow-band filter's bandpass. Since we are limiting our discussion to galaxies with narrow-band minus broad-band AB magnitudes more negative than -1.03, this approximation is certainly valid. However, we do note that by using T_C instead of $T_{\rm max}$, we are intentionally overestimating the flux and equivalent width of some galaxies, in order to minimize the errors in others. So, while the application of T_C formally translates our $\Delta m = -1.03$ criterion into a minimum emission-line equivalent width of 90 Å, galaxies with emission-lines that fall near the peak of the filter transmission function can have equivalent widths that are $\sim 12\%$ smaller. This implies that the absolute minimum equivalent width limit for our sample of LAEs is 80 Å.

2.2. Sample of LAE Candidates

Tables 2 and 3 give the coordinates of each candidate emission-line galaxy, along with its inferred monochromatic flux and equivalent width. In total, 259 objects are listed, though many are beyond the limit of our completeness. To determine this limit, we followed the procedures of Feldmeier et al. (2003) and added 1,000,000 artificial stars (2000 at a time) to our narrow-band frame. By re-running our detection algorithms on these modified frames, we were able to compute the flux level below which the object recovery fraction dropped below the 90% threshold. This value, which corresponds to a monochromatic flux of 1.5×10^{-17} ergs cm^{-2} s^{-1} ($\log F_{5000} = -16.82$) is our limiting magnitude for statistical completeness; 162 galaxies satisfy this criterion.

Before proceeding further with our analysis, we performed one additional check on our data. To eliminate obvious AGN from our sample, we cross-correlated our catalog of emission-line objects with the lists of X-ray sources found in the 1 Msec exposure of the Chandra Deep Field South (Alexander et al. 2003), and the four 250 ksec exposure of the Extended Chandra Deep Field South (Lehmer et al. 2005; Virani et al. 2006). Two of our LAE candidates were detected in the X-ray band. The first, which is our brightest Lyα emitter, has a 0.5 – 8 keV flux of 3.4×10^{-15} ergs cm^{-2} s^{-1} (i.e., $L_{\rm X} \sim 2.8 \times 10^{44}\, {h_{70}}^{-2}$ ergs s^{-1} at $z = 3.1$) and exhibits C IV emission at 1550 Å (Lira et al. 2007). The other is an interloper: a $z = 1.6$ AGN detected via its strong C III] line at 1909 Å. For the remaining 160 objects that were not detected individually in the X-ray band, we used stacking analyses to constrain their mean X-ray power output (see Lehmer et al. 2007, for details). We find that the stacked X-ray signal, which corresponds to a ~ 40 ksec effective exposure on an average LAE, does not yield a 3σ detection in any of three X-ray bandpasses (0.5–8.0 keV, 0.5–2.0 keV, and 2–8 keV). These results imply a 3σ upper-limit of $\sim 3.8 \times 10^{41}\, h_{70}^{-2}$ ergs s^{-1} on the mean 0.5–2.0 keV luminosity for our LAEs, which demonstrates that few of our Lyα sources harbor low-luminosity AGN. Similarly, if we use the conversion of Ranalli et al. (2003), we can translate this X-ray non-detection into an upper-limit for a typical LAE's star-formation rate. This limit, $85\, {h_{70}}^{-2}\, M_{\odot}$ yr^{-1}, is roughly an order of magnitude greater than the rates inferred from the objects' Lyα emission or UV continua (see Section 6).

For the remainder of this paper, we will treat our $z = 3.1$ X-ray source as AGN and exclude it from the analysis. This leaves us with a sample of 160 objects, which we assume are all star-forming galaxies. We note that, because all of our objects have equivalent widths greater than 80 Å, they are unlikely to be [O II] emitters. At $z \sim 0.34$, our survey volume is only $\sim 7300\, {h_{70}}^{-3}$ Mpc^3, which, through the luminosity functions of Hogg et al. (1998), Gallego et al. (2002), and Teplitz et al. (2003), implies a total population of between ~ 20 and ~ 200 [O II] emission-line galaxies above our completeness limit. Since less than 2%

of these objects will have rest frame equivalent widths greater than $\sim$ 60 Å (Hogg et al. 1998), the number of [O II] interlopers in our sample should be negligible. This estimate is confirmed by follow-up spectroscopy: of the 52 LAE candidates observed with sufficient signal-to-noise for a redshift determination, *all* are confirmed Lyα emitters (Gawiser et al. 2006a; Lira et al. 2007).

Figure 5 shows the spatial distribution of the LAEs above our completeness limit. The sources are obviously clustered, falling along what appear to be "walls" or "filaments". The GOODS region has a below-average number of $z = 3.1$ Lyα emitters, and there are almost no objects in the northwestern part of the field. Conversely, the density of LAEs east and northeast of the field center is quite high. This type of data can be an extremely powerful probe of cosmological history, but we will defer a discussion of this topic to a future paper (Gawiser et al. 2007).

3. The Continuum Properties of the Emitters

To investigate the continuum properties of our Lyα emitters, we measured the brightness of each LAE on the broadband UBVR images of the MUSYC survey (Gawiser et al. 2006b). Since the catalog associated with this dataset has a $5\,\sigma$ detection threshold of $U = 26.0$, $B = 26.9$, $V = 26.4$, and $R = 26.4$, our knowledge of the LAEs' positions (obtained from the narrow-band frames) allows us to perform photometry well past this limit. Figure 6 displays the $B - R$ color-magnitude diagram for 88 of the LAEs brighter than $R_{AB} = 27.25$. The diagram, which shows the galaxies' rest-frame continua at 1060 and 1570 Å, has several features of note.

The first involves the color distribution of our objects. According to the figure, LAEs with R-band magnitudes brighter than $R = 25$ have a median color of $B - R = 0.53$. This value agrees with the blue colors found by Venemans et al. (2005) for a sample of Lyα emitters at $z = 3.13$, and is the value expected for a $\sim 10^8$ yr old stellar system evolving with a constant star-formation rate (Fujita et al. 2003; Bruzual & Charlot 2003). This median color is also consistent with the results of Gawiser et al. (2006a), who stacked the broad-band fluxes of 18 spectroscopically confirmed $z = 3.1$ LAEs and showed that the typical age of these systems is between $0.01 < t < 2$ Gyr. It does, however, stand in marked contrast to the results of Stiavelli et al. (2001), who claimed that Lyα emitters at $z = 2.4$ are very red ($B - I \sim 1.8$). The blue colors of our galaxies confirm their nature as young, star-forming systems. There is no evidence for excessive reddening in these objects, and if the galaxies do possess an underlying population of older stars, the component must be quite small.

On the other hand, as the LAE color distribution indicates, Lyα emitters are not, as a class, homogeneous. At $R = 25$, the MUSYC $B - R$ colors have a typical photometric uncertainty of $\sigma_{B-R} = 0.25$ mag. This contrasts with the observed color dispersion for our galaxies, which is ~ 0.4 mag for objects with $R < 25$. Thus, there is at least a ~ 0.3 mag scatter in the intrinsic colors of these objects. Either there is some variation in the star-formation history of Lyα emitters, or dust is having an effect on the emergent colors.

Finally, it is worth emphasizing that our Lyα emitters are substantially fainter in the continuum than objects found by the Lyman-break technique. At $z \sim 3$, L^* galaxies have an apparent magnitude of $R \sim 24.5$ (Steidel et al. 1999) and ground-based Lyman-break surveys typically extend only ~ 1 mag beyond this value (see Giavalisco 2002, for a review). Furthermore, spectroscopic surveys of LBG candidates rarely target galaxies fainter than $R = 24$. In our emission-line sample, the median continuum magnitude is $R \sim 26.7$, and many of the galaxies have aperture magnitudes significantly fainter than $R \sim 28$. In general, LAEs do inhabit the same location as LBGs in the U-V vs. V-R color-color space (see Figure 7), but their extremely faint continuum sets them apart.

This is also illustrated in Figure 8, which compares the rest frame 1570 Å luminosity function of our complete sample of Lyα emitters (those with monochromatic fluxes greater than 1.5×10^{-17} ergs cm^{-2} s^{-1}) with the rest-frame 1700 Å luminosity function of $z = 3.1$ Lyman-break galaxies (Steidel et al. 1999). When plotted in this way, our sample of LAEs appears incomplete, since for $R \gtrsim 26.5$, only the brightest emission-line sources will make it into our catalog. The plot also implies that at $z = 3.1$, $R < 25.5$, Lyα emitters are ~ 3 times rarer than comparably bright Lyman-break galaxies. Since this ratio is virtually identical to that measured by Steidel et al. (2000) within an extremely rich $z = 3.09$ protocluster, this suggests that the number is not a strong function of galactic environment. But, most strikingly, our observations demonstrate the Lyα emitters sample the entire range of the (UV-continuum) luminosity function. The median UV luminosity of LAEs in our sample is $\lesssim 0.2L^*$, and the faintest galaxy in the group is no brighter than $\sim 0.02L^*$. Just as broadband observations detect all objects at the bright-end of the continuum luminosity function, but sample the entire range of emission-line strengths, our narrow-band survey finds all the brightest emission-line objects, but draws from the entire range of continuum brightness.

4. The Lyα Equivalent Width Distribution

Before examining the emission-line properties of our dataset, we need to correct for the observational biases and selection effects that are present in the sample. Since the

data were taken in a fast-beam through a filter with a non-square bandpass, these effects are substantial. Continuum measurements, of course, are unaffected by the peculiarities of a narrow-band filter, but the distribution of monochromatic fluxes can be significantly distorted. Specifically, the observed flux distribution will be the convolution of the true distribution with the following two kernels:

The Photometric Error Function: The random errors associated with our narrow-band photometry vary considerably, ranging from ~ 0.02 mag at the bright end, to ~ 0.2 mag near the completeness limit (see Table 4). These errors will scatter objects from heavily populated magnitude bins into bins with fewer objects, and flatten the slope of the luminosity function. Because the change in slope goes as the square of the measurement uncertainty (Eddington 1913, 1940), the effect of this convolution is most important for objects near the survey limit.

The Filter Transmission Function. As described in Section 2.1, the narrow-band filter used for this survey has a transmission function that is nearly Gaussian in shape. This creates an odd-shaped convolution kernel (the right panel of Figure 4), which systematically decreases the measured line-emission of objects falling away from the peak of the transmission curve. Moreover, because the objects' equivalent widths are also reduced by this bandpass effect, some fraction of the LAE population will be lost from our EW > 80 Å sample. The result is that the normalization of this filter transmission kernel is not unity. Instead, it depends on the intrinsic equivalent width distribution of the galaxies, since that is the function that defines the fraction of galaxies (at each redshift) which can still make it into our sample.

These effects are illustrated in the top panel of Figure 9, which displays a histogram of the rest-frame equivalent widths for our candidate Lyα galaxies. As the dotted line shows, the data appear to be well fit by an exponential that has an e-folding length of $w_{\rm obs} = 214^{+19}_{-15}$ Å. However, because the bandpass of our narrow-band filter is more Gaussian-shaped than square, the line-strengths of many of the galaxies have been systematically underestimated. In fact, the true distribution of equivalent widths is broader than that measured: when we perform a maximum-likelihood analysis using a series of exponential laws, convolved with the filter bandpass and photometric error kernels, we obtain a most-likely scale length of $w_{\rm obs} = 311^{+47}_{-33}$ Å, or $w_0 = 76^{+11}_{-8}$ Å in the rest frame of the sample.

Such a distribution is quite different from that reported by Malhotra & Rhoads (2002). In their survey of 150 $z = 4.5$ Lyα emitters, $\sim 60\%$ of the objects had extremely high rest-frame equivalent widths, i.e., EW$_0 > 240$ Å. Since stellar population models, such as those by Charlot & Fall (1993) cannot produce such strong line-emission, Malhotra & Rhoads (2002) postulated the presence of a top-heavy initial mass function and perhaps the existence of Population III stars. However in our sample, only 3 out of 160 LAEs ($\sim 2\%$) have observed

rest-frame equivalent widths greater than this 240 Å limit. Even when we correct for the effects of our filter's non-square bandpass, the fraction of strong line-emitters does not exceed $\sim$ 12%. This is less than the $\sim$ 20% value estimated by Dawson et al. (2004) via Keck spectroscopy of a subset of Malhotra & Rhoads (2002) objects. Thus, at least at $z \sim 3.1$, there is no need to invoke a skewed initial mass function to explain the majority of our LAEs.

The equivalent width distribution of Figure 9 also differs dramatically from that found by Shapley et al. (2003) for a sample of $z \sim 3$ Lyman-break galaxies. In their dataset, rest-frame equivalent widths e-fold with a scale-length of $\sim$ 25 Å, rather than the $\sim$ 75 Å value derived from our LAE survey. This difference is not surprising given that the former dataset is selected to be bright in the continuum, while the latter is chosen to be strong in the emission-line. Moreover, when Shapley et al. (2003) analyzed the $\sim$ 25% of Lyman-break galaxies with rest-frame equivalent widths greater than 20 Å, they found a correlation between line strength and continuum (R-band) magnitude, in the sense that fainter galaxies had higher equivalent widths. We see that same trend in our data, but it is largely the result of a selection effect. (Faint galaxies with low equivalent widths fall below our monochromatic flux limit.) A comparison of emission-line flux with equivalent width for our statistically complete sample shows no such correlation.

The lower two panels of Figure 9 demonstrate this another way. In the diagram, our sample of LAEs is divided in half, with the middle panel showing the equivalent width distribution for objects with monochromatic Lyα luminosities greater $2 \times 10^{42}\, {h_{70}}^{-2}$ ergs s^{-1}, and the bottom panel displaying the same distribution for less luminous objects. As the figure illustrates, the distribution of equivalent widths is relatively insensitive to the absolute brightness of the galaxy. To first order this is expected, since both the UV continuum and the Lyα emission-line flux are driven by star formation. However, one could imagine a scenario wherein the amount, composition, and/or distribution of dust within the brighter (presumably more-metal rich) Lyα emitters differs from that within their lower-luminosity counterparts. Since the effect of this dust on resonantly-scattered Lyα photons is likely to be different from that on continuum photons, this change in extinction can theoretically produce a systematic shift in the distribution of Lyα equivalent widths. There is no evidence for such a shift in our data; this constancy argues against the importance of dust in these objects.

5. The Lyα Emission-Line Luminosity Function

Figure 10 shows the distribution of monochromatic fluxes for our sample of emission-line galaxies. The function looks much like a power law, with a faint-end slope of $\alpha \sim -1.5$

that steepens as one moves to brighter luminosities. However, to quantify this behavior, we once again have to correct the observed flux distribution for the distortions caused by photometric errors and the non-square bandpass of the filter. In addition, we must also consider the censoring effect our equivalent width cutoff has on the data: some line emitters whose redshifts are not at the peak of the filter transmission function will fall out of our sample completely.

To deal with these effects, we fit the observed distribution of Lyα emission-line fluxes to a Schechter (1976) function via the method of maximum likelihood (e.g., Hanes & Whittaker 1987; Ciardullo et al. 1989). We applied our two convolution kernels (including the equivalent width censorship) to a series of functions of the form

$$\phi(L)d(L/L^*) \propto (L/L^*)^{\alpha}\, e^{-L/L^*} d(L/L^*) \tag{4}$$

treated each curve as a probability distribution (i.e., with a unity normalization), and computed the likelihood that the observed sample of Lyα fluxes is drawn from the resultant distribution. The results for the three parameters of this fit, α, $\log L^*$, and N, the integral of the Schechter function down to our limiting flux (in units of galaxies Mpc^{-3}), are shown in Figure 11; Table 5 lists the best-fitting parameters, along with their marginalized most-likely values and uncertainties. For completeness, Table 5 also gives the value of ϕ^* which is inferred from our most likely solution. As expected, the plots illustrate the familiar degeneracy between L^* and α: our best-fit solution has $\alpha \sim -1.5$, but if L^* is forced to brighter luminosities, α decreases. The contours also demonstrate an asymmetry in the solutions, whereby extremely bright values of L^* are included within the $3\,\sigma$ contours of probability, but faint values of the same quantity are not.

But perhaps the most interesting feature of the analysis concerns the effective volume of our survey. As in Section 2.1, the amount of space sampled by the observations depends critically on each galaxy's Lyα luminosity and equivalent width. Bright line-emitters with large equivalent widths can be identified well onto the wings of the filter, hence the survey volume associated with these objects is relatively large. Conversely, weak line-emitters, and objects with small equivalent widths can only be detected if they lie at the peak of the filter transmission curve. Thus, the survey volume for these objects is quite small. The effective volume for our observations is therefore a weighted average, which depends on the intrinsic properties of entire LAE sample.

This average can be computed from the data displayed in Figure 11. According to the figure, the space density of galaxies with emission-line brighter than 1.5×10^{-17} ergs cm^{-2} s^{-1} (i.e., $1.3\times10^{42}\,{h_{70}}^{-2}$ ergs s^{-1}) is extremely well-defined, $1.46\pm0.12\times10^{-3}\,{h_{70}}^{3}$ galaxies Mpc^{-3}. Since this measurement comes from the detection of 160 galaxies brighter than the completeness limit, the data imply an effective survey volume of $\sim 1.1\times10^{5}\ {h_{70}}^{-3}$ Mpc^3. This is *not*

the volume one would infer from the interference filter's full-width at half-maximum: it is 25% smaller, or roughly the full-width of the filter at two-thirds maximum.

This difference is illustrated in Figure 10. The points show the space density of Lyα galaxies one would derive simply by using the filter's FWHM to define the survey volume; the solid line gives the Schechter (1976) function which best fits the data. The offset between the solid line and the dashed line, which represents the function after the application of the two convolution kernels, confirms the need for careful analysis when working with narrow-band data taken through a non-square bandpass.

The results of our maximum-likelihood calculation also suggest a simple definition for the effective transmission for our filter. As described in Section 2.1, a "characteristic" transmission is needed to convert the (bandpass-dependent) AB magnitude of an individual galaxy to monochromatic Lyα flux. Rather than use the maximum transmission (which would underestimate the flux of all galaxies not at the filter peak), or adopt some complicated scheme which involves iterating on the luminosity function, one can simply choose the filter's mean transmission within some limited wavelength range. Based on the results above, the filter's full-width at two-thirds maximum seems an appropriate limit. This transmission, which is indicated by the arrow in Figure 4, is the value used to derive the fluxes and equivalent widths of Tables 2 and 3. If were to use to filter's peak transmission instead of this characteristic value, the tabulated emission-line fluxes and equivalent widths would all be $\sim 12\%$ smaller.

The error bars quoted above for the space density of Lyα emitters represent only the statistical uncertainty of the fits. They do not include the possible effects of large-scale structure within our survey volume. Specifically, if the linear bias factor for LAEs is two (see Gawiser et al. 2007, for an analysis of the objects' clustering) then the expected fluctuation in the density of Lyα emitters measured within a $\sim 10^5\ {h_{70}}^{-3}$ Mpc^3 volume of space is $\sim 30\%$. This value should be combined in quadrature with our formal statistical uncertainty.

Since Lyα galaxies have been observed at a number of redshifts, it is tempting to use our data to examine the evolution of the LAE luminosity function. Unfortunately, the samples obtained to date are not yet robust enough for this purpose. An example of the problem is shown in Figure 12, which compares our cumulative luminosity function (and our Schechter fit for $\alpha = -1.5$) to two measures of Lyα galaxies at $z = 5.7$. As the figure illustrates, there are large differences between the measurements. If the Malhotra & Rhoads (2004) luminosity function is correct, then LAEs at $z = 3.1$ are a factor of ~ 2.5 brighter and/or more numerous than their $z = 5.7$ counterparts. However, if the $z = 5.7$ LAE luminosity function of Shimasaku et al. (2006) is correct, then evolution is occurring in the opposite direction, i.e., the star-formation rate density is declining with time. Without better data,

it is difficult to derive any conclusions about the evolution of these objects.

Figure 12 also plots our data against the predictions of a hierarchical model of galaxy formation (Le Delliou et al. 2005, 2006). As this comparison demonstrates, our luminosity function for $z = 3.1$ LAEs lies slightly below that generated by theory. This is not surprising: one of the key parameters of the model, the escape fraction of Lyα photons, was set using previous estimates of the density of $z \sim 3$ LAEs. Unfortunately, these measurements were based on extremely small samples of objects, specifically, nine $z = 3.1$ emitters from Kudritzki et al. (2000) and ten $z = 3.4$ LAEs from Cowie & Hu (1998). Since these surveys inferred a larger space density of Lyα emitters than measured in this paper, a mismatch between our data and the Le Delliou et al. (2006) models is neither unexpected nor significant.

6. Star Formation Rate Density at $z \sim 3.1$

Perhaps the most interesting result of our survey comes from a comparison of the galaxies' Lyα emission with their R-band magnitudes. Both quantities measure star formation rate: Lyα via the combination of Case B recombination theory and the Hα vs. star formation relation

$$\mathrm{SFR(Ly}\alpha) = 9.1 \times 10^{-43}\, L(\mathrm{Ly}\alpha)\ M_\odot\ \mathrm{yr}^{-1} \tag{5}$$

(Kennicutt 1998; Hu, Cowie, & McMahon 1998), and R, via population synthesis models of the rest-frame UV (λ1570)

$$\mathrm{SFR(UV)} = 1.4 \times 10^{-28}\, L_\nu\ M_\odot\ \mathrm{yr}^{-1} \tag{6}$$

(Kennicutt 1998). If both of these calibrations hold for our sample of Lyα emitters, then a plot of the two SFR indicators should scatter about a one-to-one relation.

Figure 13 displays this plot. In the figure, galaxies with Lyα star-formation rates less than $\sim 1.15 M_\odot$ yr^{-1} are excluded by our 1.5×10^{-17} ergs cm^{-2} s^{-1} monochromatic flux limit, while objects with large UV star-formation rates, but weak Lyα are eliminated by our equivalent width criterion. The latter is not a hard limit, since LAE colors range from $0 \lesssim (B+V) - R \lesssim 2.5$, and it is the $B+V$ continuum that is used to define equivalent width. Nevertheless, if we adopt 1.4 as the upper limit on the median color of an Lyα emitting galaxy (i.e., $1\,\sigma$ above the median $(B+V) - R \sim 0.65$ color of the population), we obtain the dotted line shown in the figure.

Despite these selection effects, the Lyα and UV continuum star-formation rates do seem to be correlated. However, there is an offset: the rates inferred from the UV are,

on average, about three times higher than those derived from Lyα. While the Lyα SFR measurements are generally less than $10\,{h_{70}}^{-2}\,M_{\odot}$ yr^{-1}, the rest-frame UV values extend up to $\sim 50\,{h_{70}}^{-2}\,M_{\odot}$ yr^{-1}. This discrepancy has previously been seen in a sample of 20 LAEs at $z = 5.7$ (Ajiki et al. 2003), and has two possible explanations.

The most likely cause of the offset is the galaxies' internal extinction. By studying local starburst galaxies, Calzetti (2001) has shown that a system's ionized gas is typically attenuated more than its stars. In other words, while optical and IR emission-line ratios can usually be reproduced with a simple screen model, the shape of the UV continuum requires that the dust and stars be intermingled. For a self-consistent solution, Calzetti (2001) suggests

$$E(B-V)_{\rm stars} = 0.44E(B-V)_{\rm gas} \tag{7}$$

If we apply the Calzetti (2001) law to our sample of $z = 3.1$ Lyα emitters, then for the UV and Lyα star-formation rates to be equal, the extinction within our LAEs must be as shown in Figure 14. According to the figure, in most cases it only requires a small amount of dust ($E(B-V)_{\rm stars} < 0.05$) to bring the two indicators into agreement. Figure 14 also suggests that internal extinction becomes more important in the brighter galaxies. This is consistent with observations of local starburst systems (e.g., Meurer et al. 1995), and is expected if the mass-metallicity relation seen in the local universe carries over to dust content.

Alternatively, the discrepancy between the Lyα and UV continuum star-formation rates may simply be due to uncertainties in their estimators. Models which translate UV luminosity into star formation rate have almost a factor of two scatter and rely on a number of parameters, including the initial mass function and the timescale for star formation. The latter is particularly problematic. Lyα photons are produced almost exclusively by extremely young (< 30 Myr), massive ($> 10M_{\odot}$) stars which ionize their surroundings. It therefore registers the instantaneous star-formation occurring in the galaxy. Conversely, continuum UV emission (at 1570 Å) can be produced by populations as old as ~ 1 Gyr; thus, it is a time-averaged quantity. If the star-formation rate in our Lyα emitters has declined over time, then it is possible for UV measurements to systematically overestimate the present day star formation (Glazebrook et al. 1999).

If we assume that Lyα emission is an accurate measure of star-formation, then it is possible to integrate the Schechter function to estimate the total contribution of LAEs to the star-formation rate density of the $z = 3.1$ universe. We note that this procedure does carry some uncertainty. If we just consider galaxies brighter than our completeness limit (1.5×10^{-17} ergs cm^{-2} s^{-1} or $L_{\rm Ly\alpha} > 1.3 \times 10^{42}\,{h_{70}}^{-2}$ ergs s^{-1}) then the star-formation rate density associated with LAEs is $\sim 3.6 \times 10^{-3}\,h_{70}\,M_{\odot}$ yr^{-1} Mpc^{-3}, or $1.2 \times 10^{-2}\,h_{70}\,M_{\odot}$ yr^{-1} Mpc^{-3} if the internal extinction in these objects is $E(B-V)_{\rm stars} \sim 0.05$. However, to compute the

total star-formation rate density, we need to extrapolate the LAE luminosity function to fainter magnitudes, and even 160 objects is not sufficient to define α to better than $\sim 25\%$. Consequently, our data admit a range of solutions.

This is illustrated in Figure 15, which displays SFR likelihoods derived from the probabilities illustrated in Figure 11. As the figure shows, the *most likely* value for the LAE star-formation rate density of the $z = 3.1$ universe (uncorrected for internal extinction) is $6.5 \times 10^{-3}\, h_{70}\, M_\odot$ yr^{-1} Mpc^{-3}, while the *median* value of this quantity (defined as the point with equal amounts of probability above and below) is $8.6 \times 10^{-3}\, h_{70}\ M_\odot$ yr^{-1} Mpc^{-3}. Moreover, these numbers are likely to be lower limits: if the discrepancy seen in Figure 13 is due to internal extinction, then the true SFR density is probably ~ 3.5 times higher.

The numbers above indicate that at $z = 3.1$, the star-formation rate density associated with Lyα emitters is comparable to that found for Lyman-break galaxies. Before correcting for extinction, our number for the LAE star-formation rate density is $8.6 \times 10^{-3}\, h_{70}\ M_\odot$ yr^{-1} Mpc^{-3}. For comparison, the LBG star-formation rate density at $z = 3.1$ (before extinction) is $\sim 0.01\, h_{70}\, M_\odot$ yr^{-1} Mpc^{-3} (Madau et al. 1998; Steidel et al. 1999). It is true that internal extinction within Lyman-break galaxies is typically larger than it is in our LAEs, $E(B-V) \sim 0.15$ (Steidel et al. 1999). However, according to the Calzetti (2001) extinction law, the effect of dust on the emission line flux of a galaxy is much greater than that on the stellar continuum. Consequently, our dust corrected SFR density for LAEs, $\sim 0.03 h_{70}\ M_\odot$ yr^{-1} Mpc^{-3}, is $\sim 75\%$ of the LBG value. Of course, given the extrapolations and corrections required to make this comparison, this number is highly uncertain.

7. Discussion

The space density of $z = 3.1$ Lyα emitters shown in Figure 11 translates into a surface density of 4.6 ± 0.4 arcmin^{-2} per unit redshift interval above our completeness limit. This number is similar to that derived by Thommes & Meisenheimer (2005), under the assumption that the LAE phenomenon is associated with the creation of elliptical galaxies and spiral bulges. It is also consistent with the semi-analytical hierarchical structure calculations of Le Delliou et al. (2005), though the latter predict a slightly larger number of $z \sim 3$ LAEs than found in this paper. This difference is not significant, since the Le Delliou et al. (2005) models have been adjusted to match the previous small-volume Lyα surveys of Kudritzki et al. (2000) and Cowie & Hu (1998). A $\sim 30\%$ re-scaling of the escape fraction of Lyα photons solves the discrepancy, and maintains the match between the predictions and the faint-end slope of the galaxy luminosity function.

More notable is the excellent agreement between the Le Delliou et al. (2006) simulations and the observed distribution of Lyα equivalent widths (Figure 9). Both are very well-fit via an exponential with a large ($\sim$ 75 Å) scale length. Moreover, the models also predict that the scale length observed for a magnitude-limited sample of galaxies (such as that produced by the Lyman-break technique) will be much smaller than that found via an emission-line survey. This is consistent with the LBG results found by Shapley et al. (2003).

Nevertheless, we should emphasize that the LAEs detected in this survey are probably not primordial galaxies in their initial stages of star-formation. Very few of the objects have the extremely high equivalent widths calculated for stellar populations with top-heavy initial mass functions. More importantly, the scatter in the galaxies' $m_{1060} - m_{1570}$ colors, along with the offset between the Lyα and UV continuum star-formation rates, suggests that these objects possess a non-negligible amount of dust. The existence of this dust argues against the Pop III interpretation of $z \sim 3$ Lyα emitters (Jimenez & Haiman 2006).

The extremely strong line emission associated with LAEs makes these objects especially suitable for probing the evolution of galaxies and structure in the distant universe. The space density of $z = 3.1$ emitters shown in Figure 11 translates into a surface density of 4.6 ± 0.4 arcmin^{-2} per unit redshift interval above our completeness limit. This, coupled with our measured luminosity function, implies that in the absence of evolution, there are ~ 12 LAEs arcmin^{-2} brighter than 1.5×10^{-17} ergs cm^{-2} s^{-1} in the redshift range $2 < z < 4$. Wide field integral field units, such as those being designed for ESO (Henault et al. 2004) and the Hobby-Eberly Telescope (Hill et al. 2006) will therefore be able to find large numbers of Lyα emitters in a single pointing. Moreover, because the faint-end of the luminosity function is steep ($\alpha \sim -1.5$), the density of LAEs goes linearly with survey depth. Dropping the flux limit by a factor of two (to 7.5×10^{-18} ergs cm^{-2} s^{-1}) will roughly double the number of LAEs in the sample.

With an integral-field spectrograph, it is also possible to increase the sample of high-redshift galaxies by identifying objects with equivalent widths lower than our detection threshold of 80 Å ($\sim$ 20 Å in the LAE rest frame). However, the gain in doing so is likely to be small: according to Figure 9, Lyα rest-frame equivalent widths e-fold with a scale length of $\sim$ 75 Å. If this law extrapolates to weaker-lined systems, as suggested by the models of Le Delliou et al. (2006), then most Lyα emitters are already being detected, and pushing the observations to lower equivalent widths will only increase the number counts by $\sim 20\%$. Furthermore, as the data of Hogg et al. (1998) demonstrate, contamination by foreground [O II] objects increases rapidly once the equivalent width cutoff drops below $\sim$ 50 Å in the observers frame (or $\sim$ 12 Å in the rest frame of Lyα). Unless one can accept a large increase in the fraction of contaminants, surveys for high-redshift galaxies need to either stay above

this threshold, or extend to the near-IR (to detect Hβ and [O III] λ5007 in the interlopers).

We would like to thank Kathy Durrell for her assistance in reducing the data, Sean Points and Tim Abbott for their work deriving the transmission curve of the CTIO [O III] interference filter, and Cedric Lacey for providing the Le Delliou et al. (2006) models. This work was supported by NSF grants 00-71238 and 01-37927 and HST AR10324.01A. EG and JF acknowledge the support of NSF Astronomy & Astrophysics Postdoctoral Fellowships, NSF grants 02-01667 and 03-02030.

Facilities: Blanco (Mosaic)

REFERENCES

Ajiki, M., Taniguchi, Y., Fujita, S.S., Shioya, Y., Nagao, T., Murayama, T., Yamada, S., Umeda, K., & Komiyama, Y. 2003, AJ, 126, 2091

Alexander, D.M., Bauer, F.E., Brandt, W.N., Schneider, D.P., Hornschemeier, A.E., Vignali, C., Barger, A.J., Broos, P.S., Cowie, L.L., Garmire, G.P., Townsley, L.K., Bautz, M.W., Chartas, G., & Sargent, W.L.W. 2003, AJ, 126, 539

Blake, C., & Glazebrook, K. 2003, ApJ, 594, 665

Bruzual, G., & Charlot, S. 2003, MNRAS, 344, 1000

Calzetti, D. 2001, PASP, 113, 1449

Charlot, S., & Fall, S.M. 1993, ApJ, 415, 580

Ciardullo, R., Feldmeier, J.J., Krelove, K., Bartlett, R., Jacoby, G.H., & Gronwall, C. 2002, ApJ, 566, 784

Ciardullo, R., Jacoby, G.H., Ford, H.C., & Neill, J.D. 1989, ApJ, 339, 53

Cowie, L.L., & Hu, E.M. 1998, AJ, 115, 1319

Dawson, S., Rhoads, J.E., Malhotra, S., Stern, D., Dey, A., Spinrad, H., Jannuzi, B.T., Wang, J.X., & Landes, E. 2004, ApJ, 617, 707

Jimenez, R., & Haiman, Z. 2006, Nature, 440, 501

De Propris, R., Pritchet, C.J., Hartwick, F.D.A., & Hickson, P. 1993, AJ, 105, 1243

Eather, R.H., & Reasoner, D.L. 1969, Appl. Optics, 8, 227

Eddington, A.S. 1913, MNRAS, 73, 359

Eddington, A.S. 1940, MNRAS, 100, 354

Feldmeier, J.J., Ciardullo, R., Jacoby, G.H., & Durrell, P.R. 2003, ApJS, 145, 65

Fujita, S.S., Ajiki, M., Shioya, Y., Nagao, T., Murayama, T., Taniguchi, Y., Okamura, S., Ouchi, M., Shimasaku, K., Doi, M., Furusawa, H., Hamabe, M., Kimura, M., Komiyama, Y., Miyazaki, M., Miyazaki, S., Nakata, F., Sekiguchi, M., Yagi, M., Yasuda, N., Matsuda, Y., Tamura, H., Hayashino, T., Kodaira, K., Karoji, H., Yamada, T., Ohta, K., & Umemura, M. 2003, AJ, 125, 13

Gallego, J., García-Dabó, C.E., Zamorano, J., Aragón-Salamanca, A., & Rego, M. 2002, ApJ, 570, L1

Gawiser, E., van Dokkum, P.G., Gronwall, C., Ciardullo, R., Blanc, G., Castander, F.J., Feldmeier, J., Francke, H., Franx, M., Haberzettl, L., Herrera, D., Hickey, T., Infante, L., Lira, P., Maza, J., Quadri, R., Richardson, A., Schawinski, K., Schirmer, M., Taylor, E.N., Treister, E., Urry, C.M., & Virani, S.N. 2006a, ApJ, 642, L13

Gawiser, E., et al. 2006b, ApJS, 162, 1

Gawiser, E., et al. 2007, in preparation

Giacconi, R., Zirm, A., Wang, J.X., Rosati, P., Nonino, M., Tozzi, P., Gilli, R., Mainieri, V., Hasinger, G., Kewley, L., Bergeron, J., Borgani, S., Gilmozzi, R., Grogin, N., Koekemoer, A., Schreier, E., Zheng, W., & Norman, C. 2002, ApJS, 139, 369

Giavalisco, M. 2002, ARA&A, 40, 579

Giavalisco, M., et al. 2004, ApJ, 600, L93

Glazebrook, K., Blake, C., Economou, F., Lilly, S., & Colless, M. 1999, MNRAS, 306, 843

Hanes, D.A., & Whittaker, D.G. 1987, AJ, 94, 906

Hayashino, T., Matsuda, Y., Tamura, H., Yamauchi, R., Yamada, T., Ajiki, M., Fujita, S.S., Murayama, T., Nagao, T., Ohta, K., Okamura, S., Ouchi, M., Shimasaku, K., Shioya, Y., & Taniguchi, Y. 2004, AJ, 128, 2073

Henault, F., Bacon, R., Content, R., Lantz, B., Laurent, F., Lemonnier, J.-P., & Morris, S.L. 2004, in Proc. SPIE Vol. 5249, Optical Design and Engineering, ed. L. Mazuray, P.J. Rogers, & R. Wartmann (Bellingham: SPIE), 134

Hill, G.J., MacQueen, P.J., Palunas, P., Kelz, A., Roth, M.M., Gebhardt, K., & Grupp, F. 2006, New Astronomy Review, 50, 378

Hogg, D.W., Cohen, J.G., Blandford, R., & Pahre, M.A. 1998, ApJ, 504, 622

Hu, E.M., Cowie, L.L., & McMahon, R.G. 1998, ApJ, 502, L99

Jacoby, G.H., Ciardullo, R., Booth, J., & Ford, H.C. 1989, ApJ, 344, 704

Jacoby, G.H., Quigley, R.J., & Africano, J.L. 1987, PASP, 99, 672

Kennicutt, R.C. 1998, ARA&A, 36, 189

Kodaira, K., et al. 2003, PASJ, 55, L17

Koehler, R.S., Schuecker, P., & Gebhardt, K. 2007, A&A, 462, 7

Kudritzki, R.-P., Méndez, R.H., Feldmeier, J.J., Ciardullo, R., Jacoby, G.H., Freeman, K.C., Arnaboldi, M., Capaccioli, M., Gerhard, O., & Ford, H.C. 2000, ApJ, 536, 19

Le Delliou, M., Lacey, C., Baugh, C.M., Guiderdoni, B., Bacon, R., Courtois, H., Sousbie, T., & Morris, S.L. 2005, MNRAS, 357, L11

Le Delliou, M., Lacey, C.G., Baugh, C.M., & Morris, S.L. 2006, MNRAS, 365, 712

Lehmer, B.D., Brandt, W.N., Alexander, D.M., Bauer, F.E., Schneider, D.P., Tozzi, P., Bergeron, J., Garmire, G.P., Giacconi, R., Gilli, R., Hasinger, G., Hornschemeier, A.E., Koekemoer, A.M., Mainieri, V., Miyaji, T., Nonino, M., Rosati, P., Silverman, J.D., Szokoly, G., & Vignali, C. 2005, ApJS, 161, 21

Lehmer, B.D., Brandt, W.N., Alexander, D.M., Bell, E.F., McIntosh, D.H., Bauer, F.E., Hasinger, G., Mainieri, V., Miyaji, T., Schneider, D.P., & Steffen, A.T. ApJ, 657, 681

Lira, P., et al. 2007, in preparation

Madau, P., Ferguson, H.C., Dickinson, M.E., Giavalisco, M., Steidel, C.C., & Fruchter, A. 1996, MNRAS, 283, 1388

Madau, P., Pozzetti, L., & Dickinson, M. 1998, ApJ, 498, 106

Malhotra, S., & Rhoads, J.E. 2002, ApJ, 565, L71

Malhotra, S., & Rhoads, J.E. 2004, ApJ, 617, L5

Meier, D.L., & Terlevich, R. 1981, ApJ, 246, L109

Meurer, G.R., Heckman, T.M., Leitherer, C., Kinney, A., Robert, C., & Garnett, D.R. 1995, AJ, 110, 2665

Monet, D., Bird, A., Canzian, B., Dahn, C., Guetter, H., Harris, H., Henden, A., Levine, S., Luginbuhl, C., Monet, A.K.B., Rhodes, A., Riepe, B., Sell, S., Stone, R., Vrba, F., & Walker, R. 1998, PMM USNO-A2.0: A Catalogue of Astrometric Standards (Washington, DC: US Naval Obs.)

Ouchi, M., Shimasaku, K., Furusawa, H., Miyazaki, M., Doi, M., Hamabe, M., Hayashino, T., Kimura, M., Kodaira, K., Komiyama, Y., Matsuda, Y., Miyazaki, S., Nakata, F., Okamura, S., Sekiguchi, M., Shioya, Y., Tamura, H., Taniguchi, Y., Yagi, M., & Yasuda, N. 2003, ApJ, 582, 60

Ranalli, P., Comastri, A., & Setti, G. 2003, A&A, 399, 39

Rhoads, J.E., Dey, A., Malhotra, S., Stern, D., Spinrad, H., Jannuzi, B.T., Dawson, S., Brown, M., & Landes, E. 2003, AJ, 125, 1006

Rhoads, J.E., Malhotra, S., Dey, A., Stern, D., Spinrad, H., & Jannuzi, B.T. 2000, ApJ, 545, L85

Rix, H.-W., Barden, M., Beckwith, S.V.W., Bell, E.F., Borch, A., Caldwell, J.A.R., Häussler, B., Jahnke, K., Jogee, S., McIntosh, D.H., Meisenheimer, K., Peng, C.Y., Sanchez, S.F., Somerville, R.S., Wisotzki, L., & Wolf, C. 2004, ApJS, 152, 163

Schechter, P. 1976, ApJ, 203, 297

Seo, H.-J., & Eisenstein, D.J. 2003, ApJ, 598, 720

Shapley, A.E., Steidel, C.C., Pettini, M., & Adelberger, K.L. 2003, ApJ, 588, 65

Shimasaku, K., Hayashino, T., Matsuda, Y., Ouchi, M., Ohta, K., Okamura, S., Tamura, H., Yamada, T., & Yamauchi, R. 2004, ApJ, 605, L93

Shimasaku, K., Kashikawa, N., Doi, M., Ly, C., Malkan, M.A., Matsuda, Y., Ouchi, M., Hayashino, T., Iye, M., Motohara, K., Murayama, T., Nagao, T., Ohta, K., Okamura, S., Sasaki, T., Shioya, Y., & Taniguchi, Y. 2006, PASJ, 58, 313

Steidel, C.C., Adelberger, K.L., Giavalisco, M., Dickinson, M., & Pettini, M. 1999, ApJ, 519, 1

Steidel, C.C., Adelberger, K.L., Shapley, A.E., Pettini, M., Dickinson, M., & Giavalisco, M. 2000, ApJ, 532, 170

Steidel, C.C., Adelberger, K.L., Shapley, A.E., Pettini, M., Dickinson, M., & Giavalisco, M. 2003, ApJ, 592, 728

Steidel C.C., Giavalisco, M., Dickinson, M., & Adelberger, K.L. 1996a, AJ, 112, 352

Steidel, C.C., Giavalisco, M., Pettini, M., Dickinson, M., & Adelberger, K.L. 1996b, ApJ, 462, L17

Stiavelli, M., Scarlata, C., Panagia, N., Treu, T., Bertin, G., & Bertola, F. 2001, ApJ, 561, L37

Stone, R.P.S. 1977, ApJ, 218, 767

Taniguchi, Y., et al. 2005, PASJ, 57, 165

Tapken, C., Appenzeller, I., Gabasch, A., Heidt, J., Hopp, U., Bender, R., Mehlert, D., Noll, S., Seitz, S., & Seifert, W. 2006, A&A, 455, 145

Teplitz, H.I., Collins, N.R., Gardner, J.P., Hill, R.S., & Rhodes, J. 2003, ApJ, 589, 704

Thommes, E., & Meisenheimer, K. 2005, A&A, 430, 877

Thompson, D., Djorgovski, S., & Trauger, J. 1995, AJ, 110, 963

Venemans, B.P., Röttgering, H.J.A., Miley, G.K., Kurk, J.D., de Breuck, C., Overzier, R.A., van Breugel, W.J.M., Carilli, C.L., Ford, H., Heckman, T., Pentericci, L., & McCarthy, P. 2005, A&A, 431, 793

Virani, S.N., Treister, E., Urry, C.M., & Gawiser, E. 2006, AJ, 131, 2373

Table 1. Log of Narrow-band Observations

UT Date	Exposure (hr)	Seeing (″)	Active CCDs
6 Oct 2002	2.0	1.4	8
12 Oct 2002	1.7	0.9	8
4 Jan 2003	2.0	1.0	8
5 Jan 2003	3.0	1.0	8
6 Jan 2003	3.0	1.1	8
29 Nov 2003	2.5	1.0	7
1 Dec 2003	1.7	0.9	7
23 Jan 2004	2.3	1.3	7
24 Jan 2004	2.0	0.9	7
25 Jan 2004	2.5	1.1	7
16 Feb 2004	1.1	1.0	7
17 Feb 2004	0.8	1.1	7
18 Feb 2004	1.3	1.0	7
19 Feb 2004	1.2	0.9	7
20 Feb 2004	0.9	1.0	7

Table 2. Candidate Lyα Emitters: The Statistically Complete Sample

ID	α(2000)	δ(2000)	Log F_{5000}	Equivalent Width
1[a]	03:33:16.86	−28:01:05.2	−15.596	449
2	03:33:12.72	−27:42:47.1	−15.832	392
3[b]	03:33:07.61	−27:51:27.0	−15.860	92
4	03:32:18.79	−27:42:48.3	−15.888	251
5	03:32:47.51	−27:58:07.6	−15.956	235
6	03:32:52.68	−27:48:09.4	−15.960	272
7	03:31:44.99	−27:35:32.9	−15.972	248
8	03:31:54.89	−27:51:21.0	−15.988	310
9	03:31:40.16	−28:03:07.5	−16.040	116
10	03:33:22.45	−27:46:36.9	−16.080	143

[a]Candidate AGN

[b]Foreground AGN

Table 3. Candidate Lyα Emitters: Objects Beyond the Completeness Limit

ID	α(2000)	δ(2000)	Log F_{5000}	Equivalent Width
163	03:33:14.82	−27:44:09.1	−16.824	380
164	03:32:08.46	−27:48:43.5	−16.824	445
165	03:33:26.22	−27:46:09.0	−16.824	468
166	03:33:11.73	−27:46:51.7	−16.828	312
167	03:31:26.49	−27:50:34.3	−16.828	209
168	03:33:05.64	−27:52:47.2	−16.828	284
169	03:31:50.46	−27:41:15.2	−16.828	364
170	03:33:17.68	−27:45:44.5	−16.832	109
171	03:31:48.98	−27:53:38.7	−16.832	322
172	03:33:10.77	−27:52:41.4	−16.836	356

Table 4. Photometric Uncertainties

Log F_{5000}	σ (mag)	Log F_{5000}	σ (mag)
−15.30	0.022	−16.20	0.065
−15.40	0.024	−16.30	0.073
−15.50	0.026	−16.40	0.082
−15.60	0.031	−16.50	0.104
−15.70	0.033	−16.60	0.125
−15.80	0.038	−16.70	0.158
−15.90	0.042	−16.80	0.204
−16.00	0.050	−16.90	0.264
−16.10	0.058	−17.00	0.329

Table 5. Schechter Function Parameters

Parameter	Best Solution	Marginalized Values
Log L/L^* (ergs s^{-1})	42.66	$42.64^{+0.26}_{-0.15}$
α	-1.36	$-1.49^{+0.45}_{-0.34}$
$N(> 1.3 \times 10^{42}\, {h_{70}}^{-2}$ ergs s^{-1}) Mpc^{-3}	1.46×10^{-3}	$1.46^{+0.14}_{-0.11} \times 10^{-3}$
ϕ^* (Mpc^{-3})	1.28×10^{-3}	...

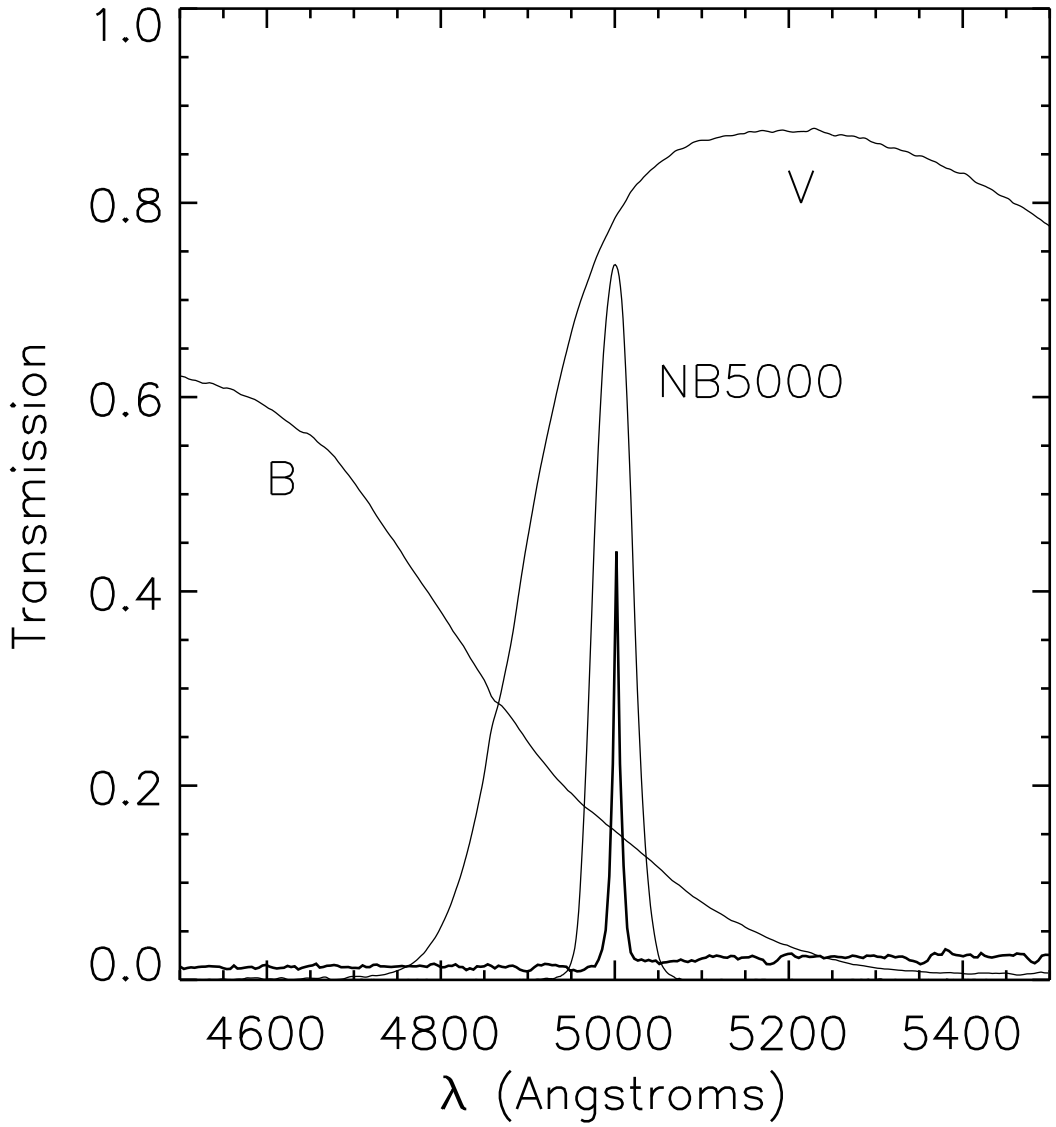

Fig. 1.— The bandpass of our narrow-band λ5000 filter, along with those of the B and V filters, which are used to define the continuum. A spectrum of a typical $z = 3.1$ Lyα galaxy is overlaid for comparison. Our narrow-band filter isolates the emission line of Lyα sources with $3.09 \lesssim z \lesssim 3.13$.

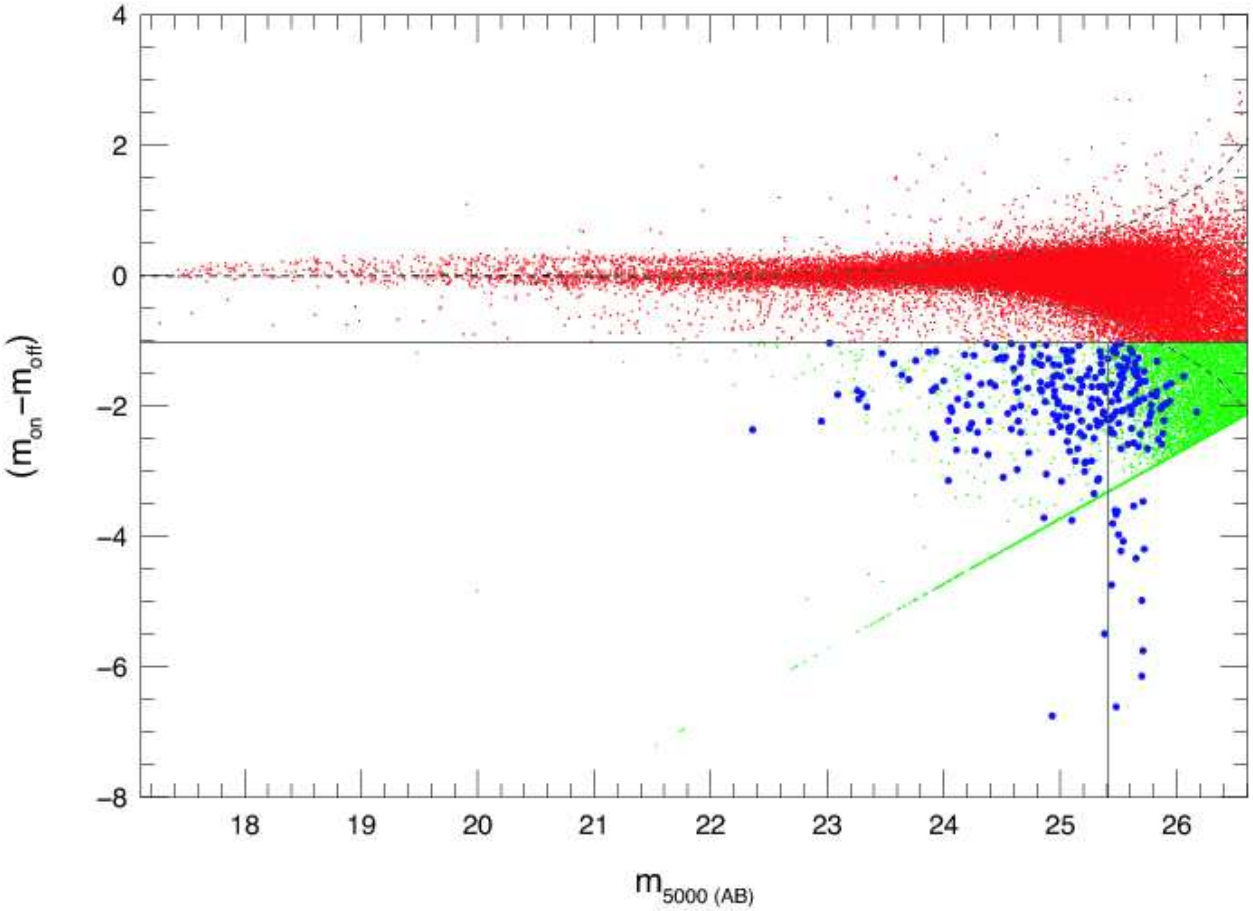

Fig. 2.— Excess emission in the narrow-band λ5000 filter over the continuum for objects in our survey field. The abscissa gives the instrumental λ5000 magnitude, while the ordinate shows the difference between the sources' narrow-band and $B+V$ continuum AB magnitudes. Our narrow-band completeness limit of 1.5×10^{-17} ergs cm^{-2} s^{-1} is represented by a vertical line; our equivalent width limit of 90 Å is shown via the horizontal line. The curve shows the expected $1\,\sigma$ errors in the photometry. Candidate emission line galaxies are denoted as blue circles; the green dots indicate LAE candidates found by our detection algorithms, but rejected upon visual inspection.

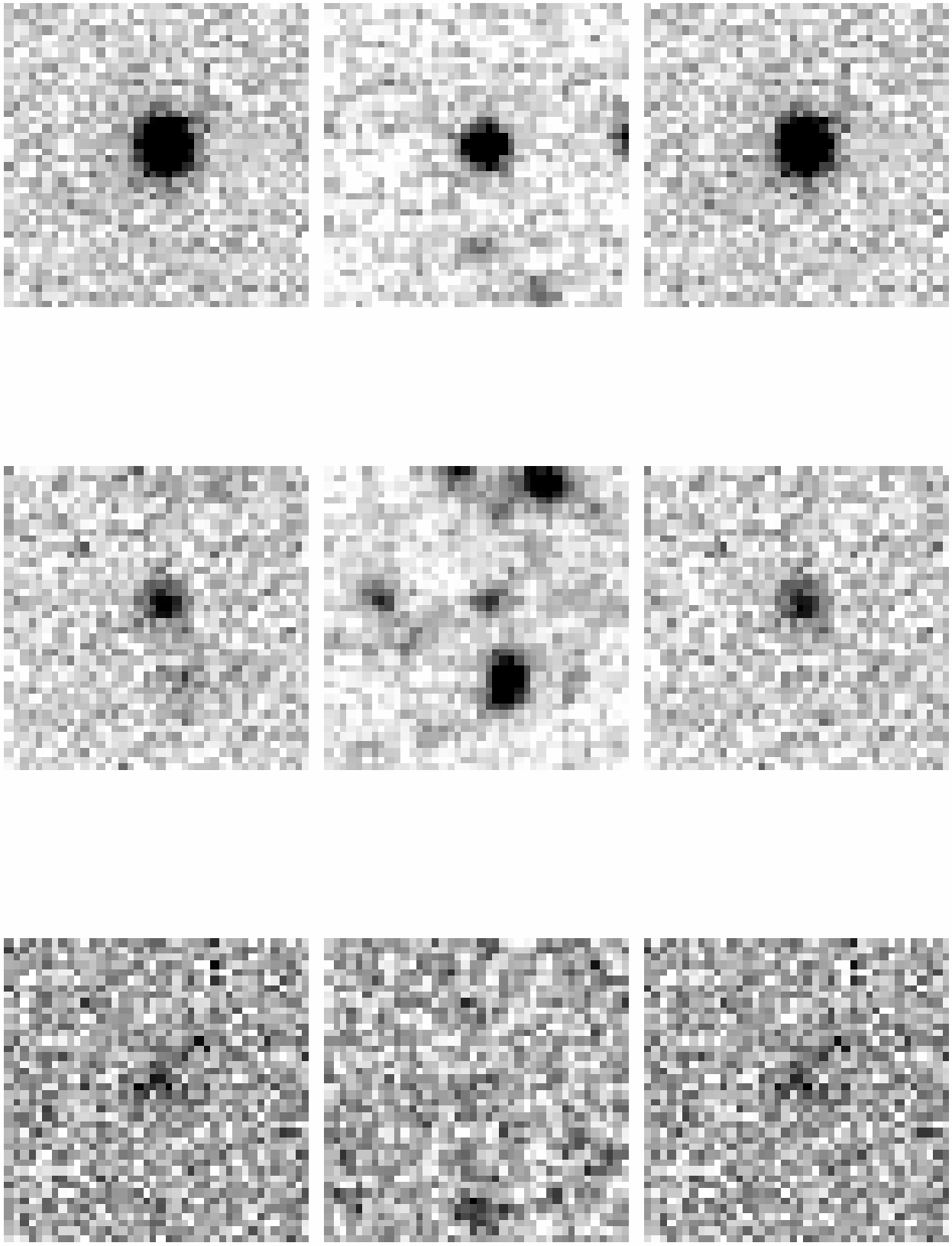

Fig. 3.— Narrow-band $\lambda 5000$, $B+V$, and difference images for three candidate emission-line galaxies. Each frame is $10''$ on a side, with north up and east to the left. The objects span a range of brightness from $\log F_{5000} = -15.60$ at the top to $\log F_{5000} = -16.74$ at the bottom.

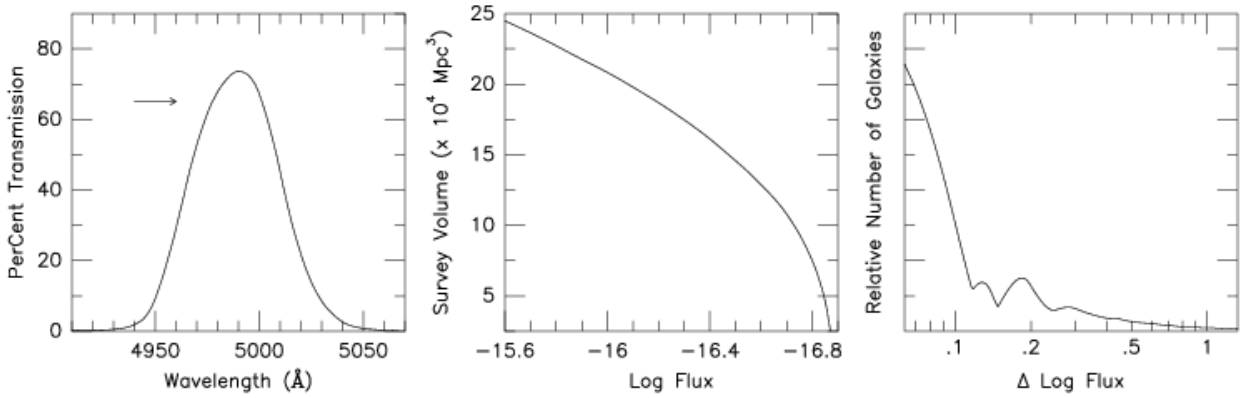

Fig. 4.— The left-hand panel shows the transmission curve for our narrow-band λ5000 filter at the outside ambient temperature and in the converging f/3.2 beam of the 4-m telescope. Note that the bandpass is nearly Gaussian in shape. The arrow shows the transmission value used to translate AB magnitude into monochromatic flux (see text). The center panel uses the transmission function to illustrate how our survey volume changes with emission-line sensitivity. The right-hand panel translates the transmission function into the photometric convolution kernel that is described in the text.

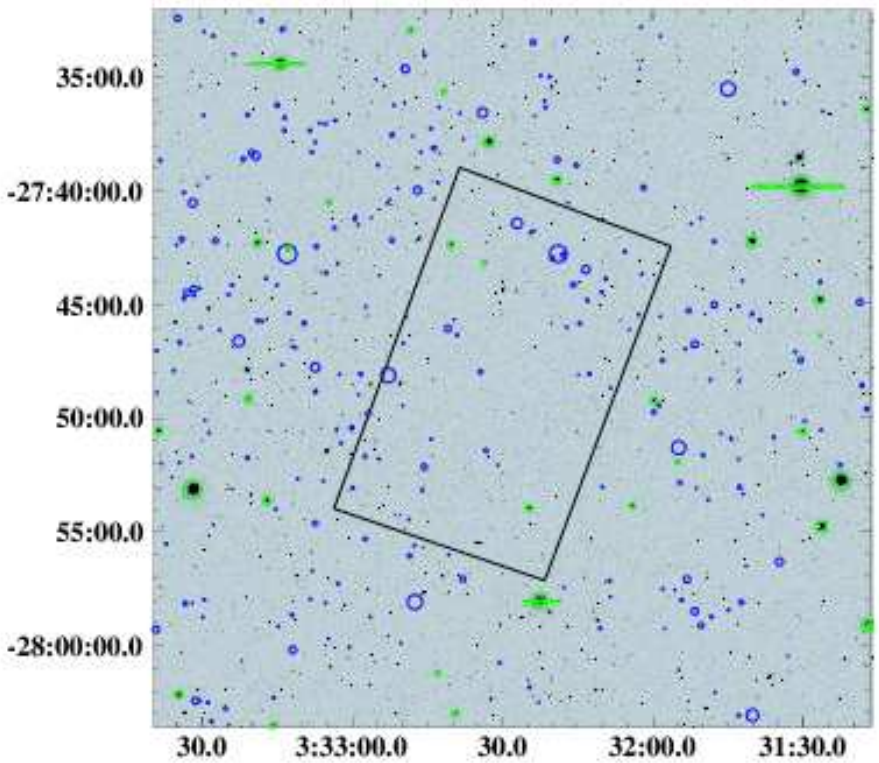

Fig. 5.— The sky coordinates of the 160 candidate $z = 3.1$ LAEs brighter than our completeness limit plotted over our narrow-band 5000 Å image. The size of each circle is proportional to Lyα luminosity, with the largest circle representing $1.25 \times 10^{43}\, {h_{70}}^{-2}$ ergs s^{-1}. The green regions show areas of the chip near bright stars that were excluded from the analysis; the large rectangle is the GOODS field.

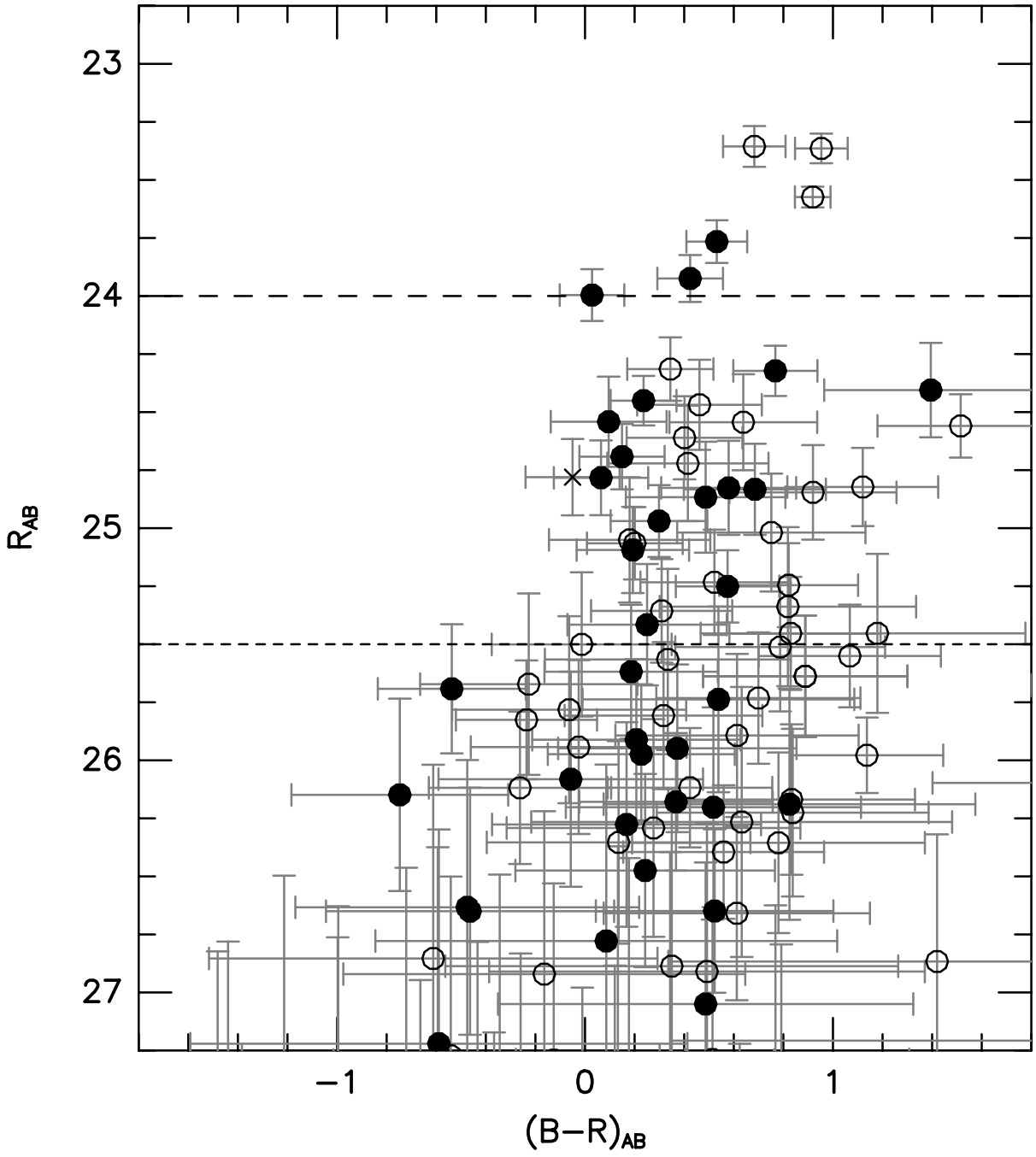

Fig. 6.— The $B - R$ (rest frame $m_{1060} - m_{1570}$) color-magnitude diagram for LAEs. The solid circles represent galaxies which have been spectroscopically confirmed as Lyα emitters (Lira et al. 2007); the cross indicates the lone AGN. The long-dashed line at $R = 24$ represents the typical magnitude limit of LBG spectroscopic surveys; the short-dashed line at $R = 25.5$ gives the photometric limit of most LBG observations. Note that the median color of our LAEs is quite blue; this is consistent with models for galaxies with recent star formation. Note also the large range of colors displayed in the figure. This scatter is greater than that expected from the photometric errors, and suggests that the LAE population is not homogeneous.

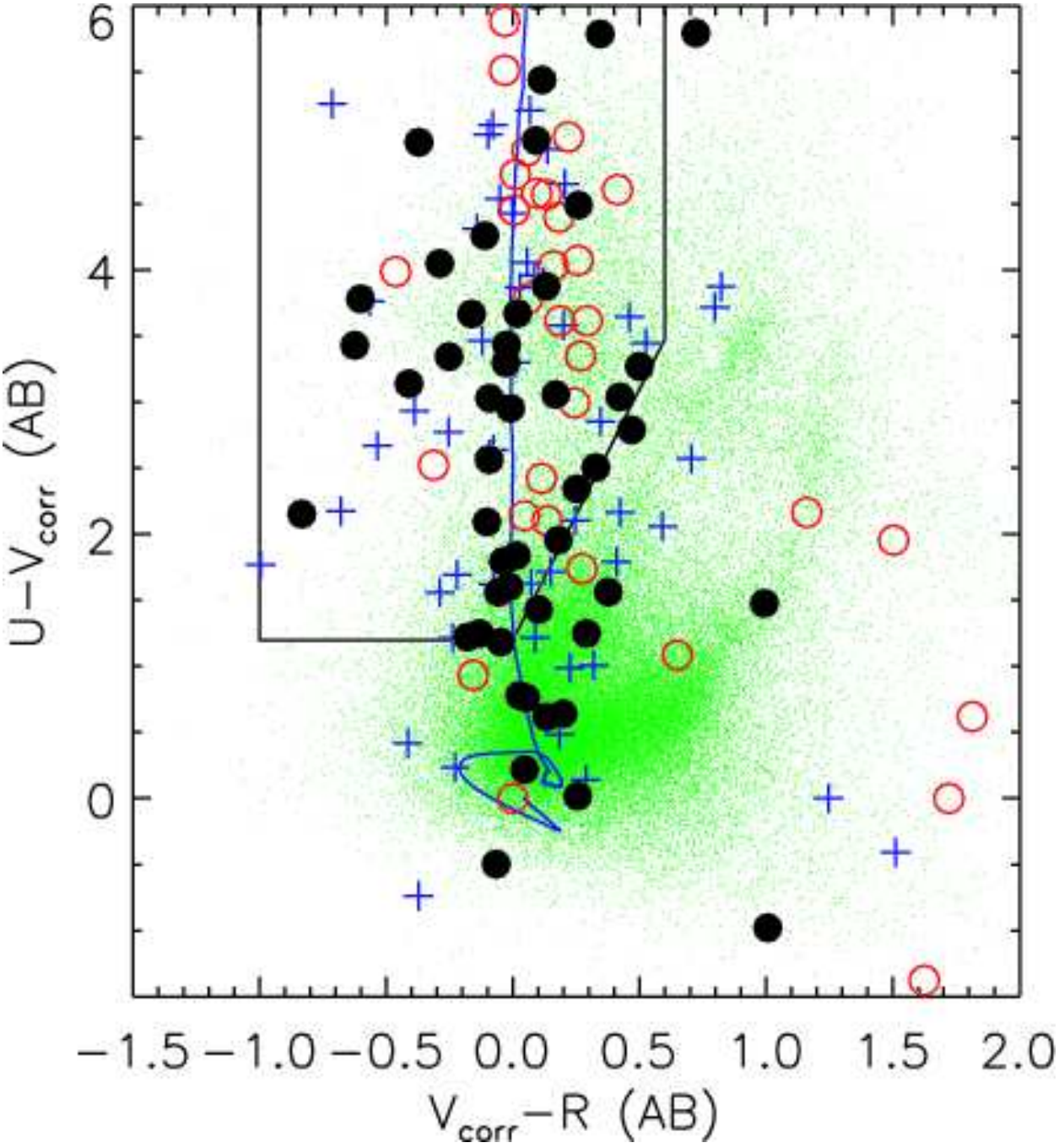

Fig. 7.— The $U-V$ versus $V-R$ colors of our $z=3.1$ LAEs. The solid circles show spectroscopically confirmed LAEs, the open circles represent sources observed with insufficient signal-to-noise for classification, and the crosses are objects with no spectroscopy. The dots are the entire 84,410 object catalog. The polygon is the LBG selection region; the sold curve is the track of an LBG template spectrum. This track falls inside the selection region in the redshift range $2.8 < z < 3.4$ (Shapley et al. 2003). Although most LAEs have LBG-like colors, their $R > 25.5$ magnitudes exclude them from the "spectroscopic" samples studied by Steidel et al. (1996a,b, 2003). The contribution of each LAE's emission line to its V-band flux has been subtracted to yield V_{corr}.

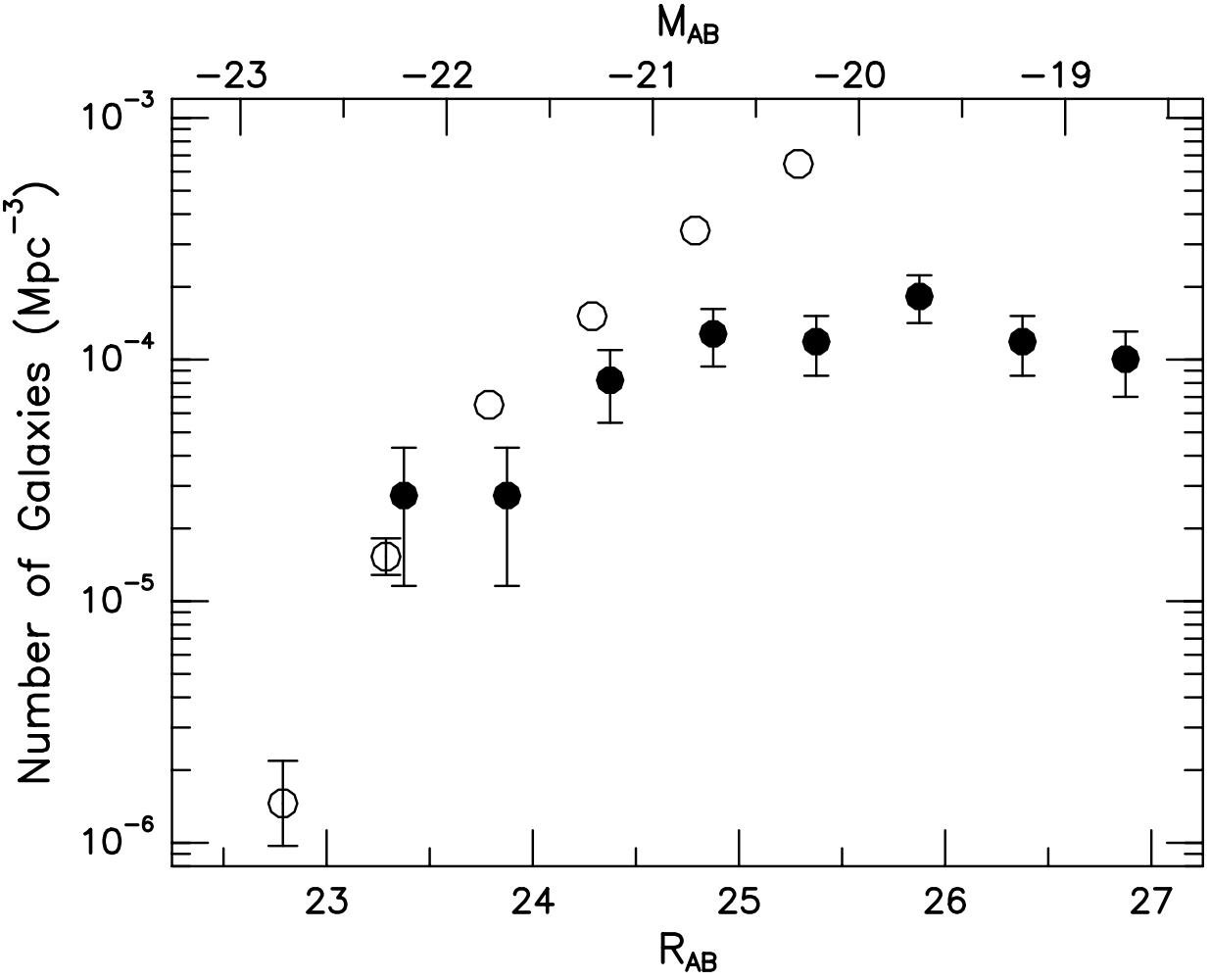

Fig. 8.— The R_{AB} (rest frame 1570 Å) luminosity function of our $z = 3.1$ Lyα emitters (solid circles), compared to the rest-frame 1700 Å luminosity function of $z = 3.04$ Lyman-break galaxies (open circles) from (Steidel et al. 1999). The flattening of our luminosity function at $R > 26.5$ is due to selection: at these magnitudes, only the strongest line emitters make it into our sample. In the magnitude range $R < 25.5$, $z = 3.1$ Lyα emitters are ~ 3 times rarer than Lyman-break galaxies.

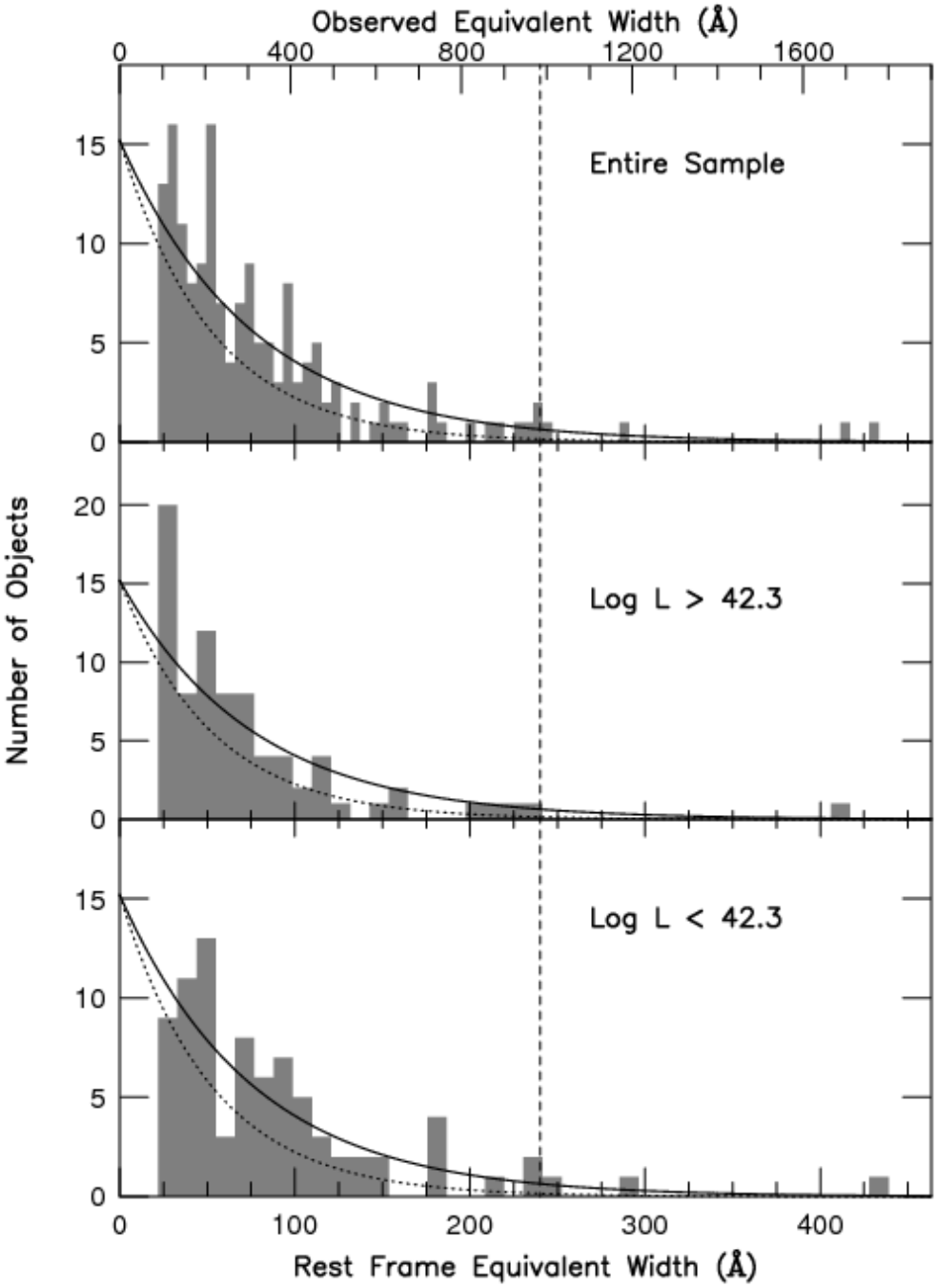

Fig. 9.— The top panel shows the observed distribution of equivalent widths for all the Lyα emission-line galaxies in our sample. The dotted line shows the apparent best-fit exponential for the distribution; the solid curve shows the exponential after correcting for the effects of photometric error and our filter's non-square transmission curve. The lower two panels divide the sample in half, and demonstrate that the exponential law does not change much with galaxy luminosity. The vertical dashed line shows the maximum equivalent width expected for populations with normal initial mass functions.

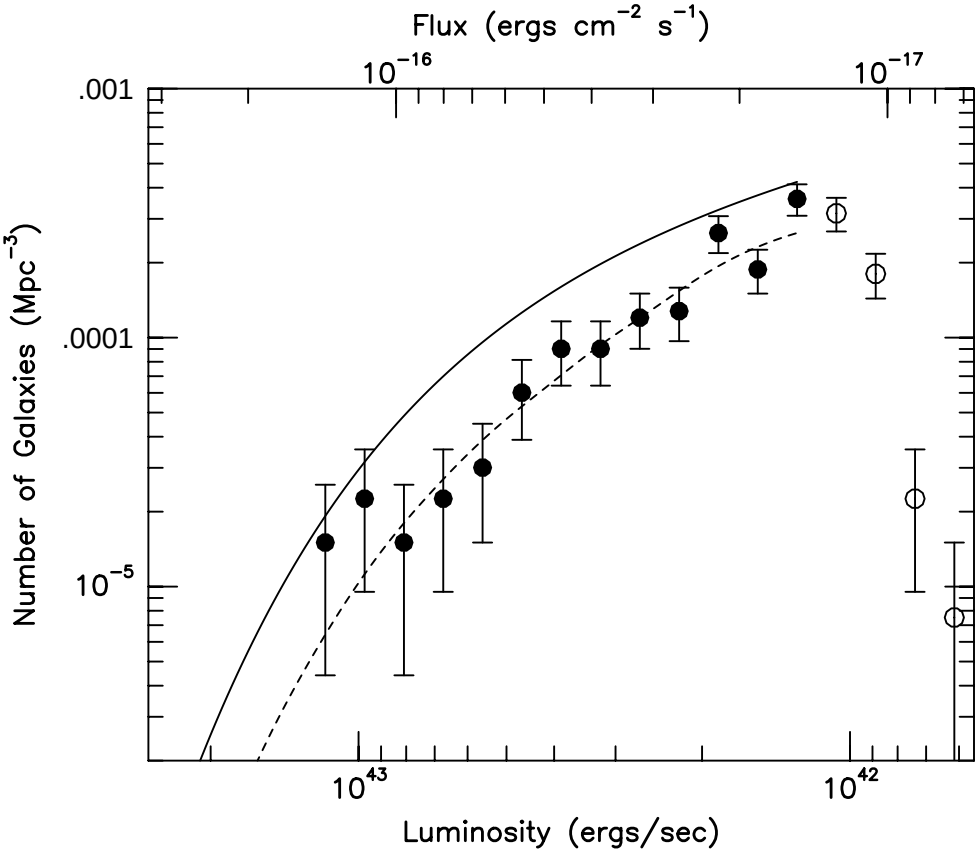

Fig. 10.— The number density of $z = 3.1$ Lyα galaxies with observers' frame equivalent widths greater than 90 Å binned into 0.2 mag intervals. The points give the density of objects under the assumption that our filter's FWHM defines the survey volume; the open circles represent data beyond our completeness limit. The solid curve shows our input best-fit Schechter (1976) luminosity function, while the dashed line illustrates the shape and normalization of this function after correcting for the effects of photometric error and our filter's non-square transmission curve.

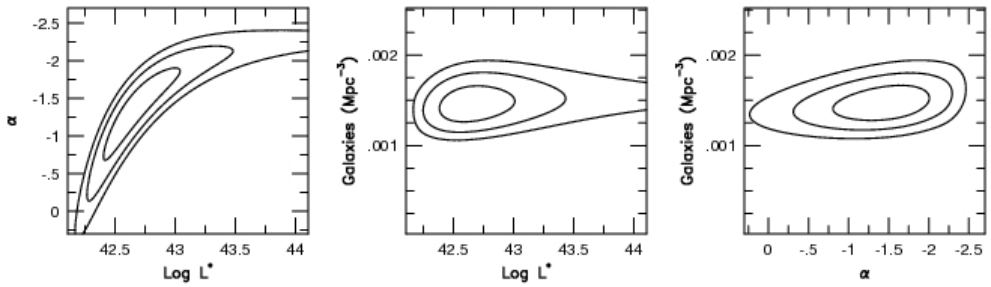

Fig. 11.— Maximum likelihood confidence contours for our Schechter (1976) function fit to the observed distribution of Lyα fluxes. The three parameters in the analysis are the faint-end slope (α), the bright-end cutoff ($\log L^*$) and the space density of galaxies with observed monochromatic fluxes greater than 1.5×10^{-17} ergs cm^{-2} s^{-1}, i.e., $L_{\mathrm{Ly}\alpha} > 1.3 \times 10^{42}\, {h_{70}}^{-2}$ ergs s^{-1}. The contours of probability are drawn at $1\,\sigma$ intervals.

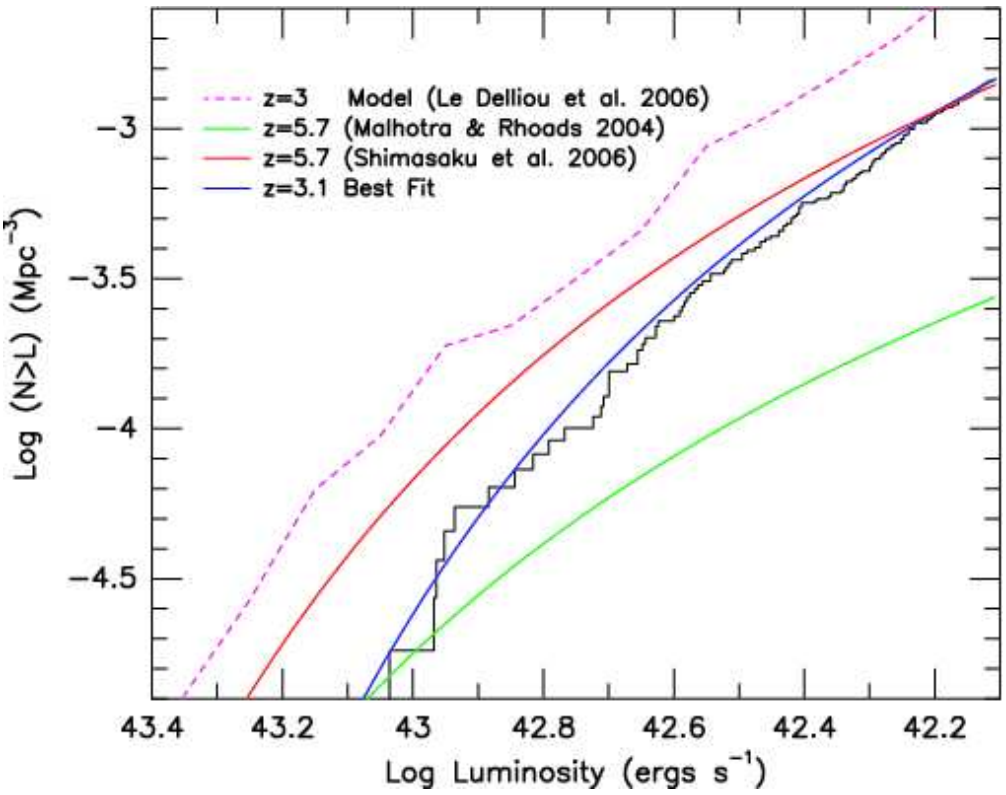

Fig. 12.— The cumulative Lyα luminosity function inferred from our survey of Lyα emitters with rest-frame equivalent widths greater than 22 Å. The solid blue line shows our best fit Schechter (1976) function ($\alpha = -1.49$), the green line is the $\alpha = -1.5$ luminosity function found by Malhotra & Rhoads (2004) for LAEs at $z = 5.7$, and the red line is the Schechter fit for $z = 5.7$ emitters found by Shimasaku et al. (2006). The dashed line is Model A by Le Delliou et al. (2006). For purposes of this figure, our data have been artificially normalized to match our best-fit function. The large difference between the Malhotra & Rhoads (2004) and Shimasaku et al. (2006) fits makes it impossible to study the evolution of the LAE population at this time.

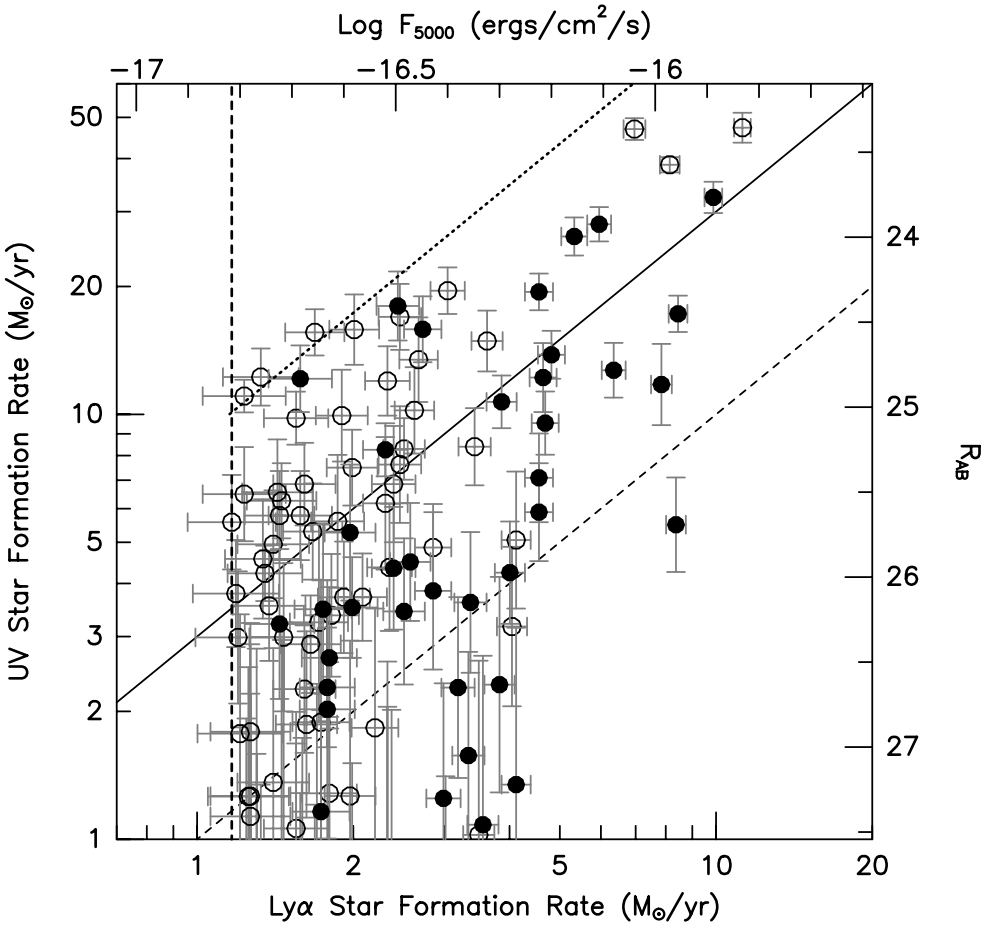

Fig. 13.— A comparison of the star formation rates derived from Lyα emission (under Case B recombination) and the UV continuum at 1570 Å. The solid dots represent spectroscopically confirmed objects (Lira et al. 2007). The diagonal dashed line shows where the two measurements are equal, while the solid line illustrates where the UV continuum star-formation rate is three times the Lyα rate. Our flux limit is shown via the vertical dashed line; the approximate location of our equivalent width threshold is shown via the dotted line (see text). Note that, although the two indicators are correlated, the Lyα-inferred rates are ~ 3 times less than those derived from the UV continuum.

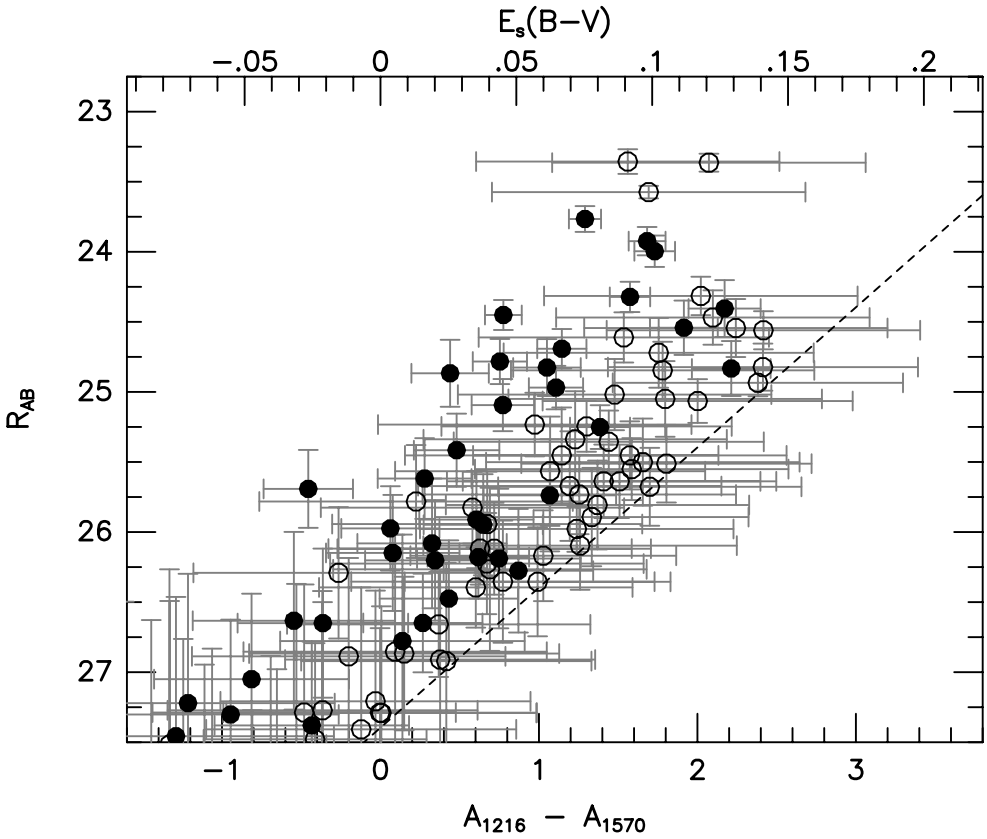

Fig. 14.— Estimates of the internal extinction within our Lyα emitters, formed using the assumption that the galaxies' ionized gas is attenuated more than its stars (Calzetti 2001). The solid dots represent spectroscopically confirmed Lyα emitters; the dashed line shows the monochromatic flux limit of our survey. Note that very little internal extinction is needed to bring the UV and Lyα star-formation rates into agreement: even in the bright ($R > 24.5$) galaxies, the internal extinction is never more than $E(B-V)_{\rm stars} \sim 0.1$.

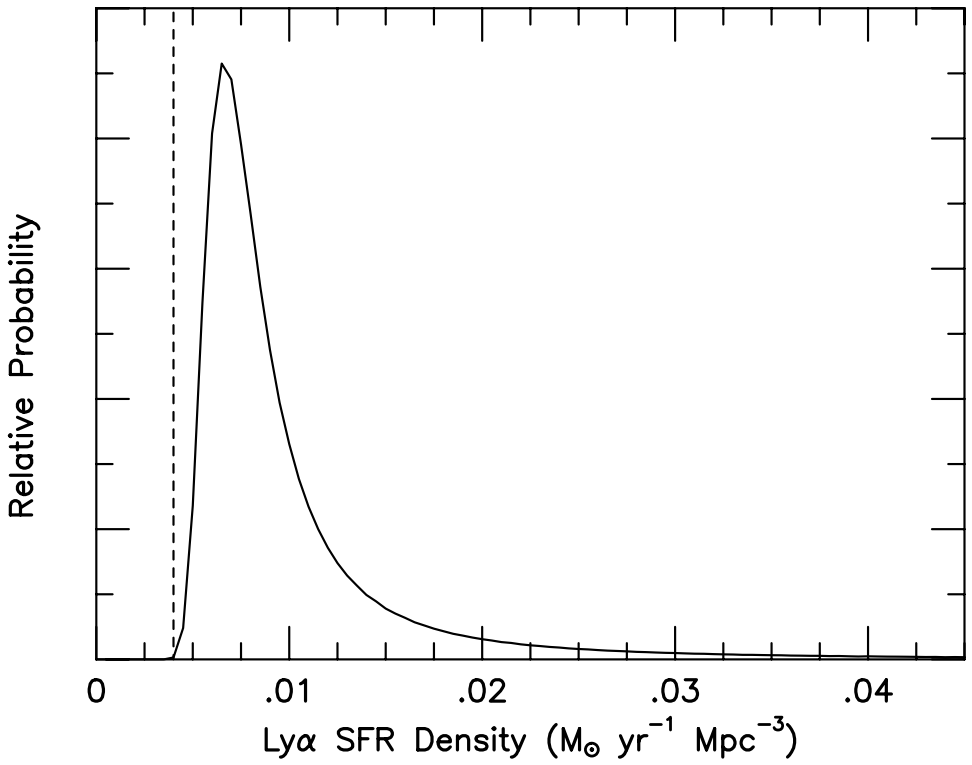

Fig. 15.— The results of our maximum likelihood analysis for the contribution of Lyα emitters to the star formation rate density of the universe. The abscissa is the star formation rate density derived from the observed luminosity of the Lyα emission line; the ordinate is the relative probability of a solution. The dashed line shows the *observed* star formation rate density associated with galaxies above our completeness limit, i.e., without any extrapolation of the galaxy luminosity function. No correction for internal extinction has been applied. The figure implies that the amount of star formation taking place in galaxies with strong Lyα emission is comparable to that in Lyman-break galaxies.